CHAPTER 5

Physical, Structural, Thermal and Electrical Properties of

$x(NaI):(100-x)[30Na_2O:(56B_2O_3+14P_2O_5)]$ glass series

5.1 Introduction to the Glass Series

In addition to the halide salt LiI concentration discussed in chapter 4 for lithium borophosphate glasses, doping sodium halide salt into sodium borophosphate glasses can be a promising strategy for tailoring the electrical, thermal, and mechanical properties of these glasses, which could be useful in various applications such as in solid-state batteries, electrochemical sensors, and optoelectronic devices.

Sodium borophosphate glass has been chosen for the study because it outperforms sodium borate and phosphate glasses in terms of its properties. Sodium phosphate glass is known for its low chemical durability due to its hygroscopic nature, while sodium borate glass has a low thermal expansion coefficient [1], [2]. The investigation of the effect of halide dopant concentration on the glass structure is important because it can affect the properties of glass such as its electrochemical, optical, and electrical properties. The study of sodium ion mobility and electrical conductivity is also significant because it can provide insights into the potential use of glass in electronic and electrochemical applications.

The chosen study aims to provide a better understanding of the properties of the glass system with the composition $NaI - Na_2O - (B_2O_3 : P_2O_5)$ and its potential applications in various fields. In summary, the use of mixed glass formers in the composition of a glass skeleton can lead to improved cationic diffusion and result in properties such as high ionic conductivity and superior thermal stability. Specifically, sodium ion conducting borophosphate glasses have demonstrated excellent ionic conductivity, thermal stability, and electrochemical stability, making them a promising material for use in solid-state batteries [3]–[6].

In the sodium borophosphate glass system, the presence of BO_4 tetrahedral causes the formation of $B - O - P$ bridges, which finally yields the borophosphate glass network branches out randomly and makes it more compact [7]. The structural analysis of the sodium borophosphate glass system with composition $Na_2O - (B_2O_3 : P_2O_5)$ indicates the presence of several structural groups, including BPO_4 and BO_4, which are advantageous for ionic conduction. Moreover, the structural alteration of the network, specifically as a function of the borate component of the network former, has been associated with the observed variation in glass transition temperature with composition [8]. In the sodium borophosphate ternary glass system, the coulombic interactions between the ions are weak, it becomes easier for the sodium ions to move through the glass structure, which results in an increase in the ionic conductivity of the glass and the activation energy required for the

movement of sodium ions is also reduced which means it becomes easier for the sodium ions to move through the glass structure, which contributes to the increase in ionic conductivity. According to Mizerakova, the activation energy of the sodium borophosphate ternary glass system is at its lowest when the coulombic contact between ions is at its weakest [9]. This suggests that the conductivity of the system is influenced by the strength of the coulombic interactions between the ions. Additionally, Eichinger studied the sodium cation conductivity in a glass system composed of sodium ortho- and di-phosphate, and boric acid, which likely provides further insight into the factors that influence the conductivity of the sodium borophosphate ternary glass system [10]. Furthermore, the presence of $NaCl$ additives in sodium borate glasses has been reported to affect the ion conduction mechanism. This suggests that the conductivity of the glass system can be influenced by the presence of other compounds in the system, and that the composition of the glass can be optimized to achieve desired conductivity properties [1].

The glass system $P_2O_5 - B_2O_3 - Na_2O$ is evaluated in terms of increasing B_2O_3 content and lowering Na_2O, which exhibits increasing thermal stability and bond strength due to the creation of $B - O - P$ bonds (cross-linking) but decreases its hygroscopic nature [11]. The coulomb trapping effects of the charges are associated with the various glass-forming units, which play the determining role in comprehending the Mixed Glass Former Effect (MGFE) in $Na_2O - P_2O_5 - B_2O_3$ glass system [12]. The formation of the $B - O - P$ link in the $M_2O - P_2O_5 - B_2O_3; M = Li/Na/Cs$ glass system indicates the strong preference for heteroatomic $B - O - P$ links compare to homoatomic $P - O - P$ and $B - O - B$ couplings, according to Dirk Larink [13]. The gradual replacement of Na_2O with Na_2SO_4 in sodium sulfo-borophosphate glass causes structural changes that lead to the formation of non-bridging oxygen (NBO) sites at the expense of bridging oxygen (BO) sites. This, in turn, causes depolymerization of the phosphate network from 3-dimensional PO_4 tetrahedra to trigonal PO_3 units in a linear chain [14], [15]. However, the literature survey indicates that there has been limited investigation into the ion conductivity and relaxation mechanism in halide-doped Boro-Phosphate glass systems. Therefore, further research may be necessary to better understand the effects of Na_2SO_4 and other additives on the conductivity and relaxation behavior of these glasses.

Therefore, a research study that aims to investigate the electrical conductivity and relaxation mechanisms of a borophosphate glass system that has been modified with sodium oxide (Na_2O) and doped with sodium iodide (NaI). The study likely involves

measuring the electrical properties of the glass using various experimental techniques, such as impedance spectroscopy, to understand how the addition of Na_2O and NaI affects the flow of sodium ions within the glass. The goal of the study may be to improve our understanding of how glass conductivity can be tailored for specific applications, such as in energy storage devices or optoelectronics.

Present chapter focuses on sodium borophosphate glasses with varying compositions, where the amount of NaI is progressively increased by $x\ (wt.\%) = 1, 2.5, 4, 5, 10, 15$ and 20 in a composition $x(NaI):(100-x)[30Na_2O:(56B_2O_3+14P_2O_5)]$. The composition of each sample is denoted as $NBPx$, where x represents the weight percentage of NaI in the sample. The samples were prepared and subjected to electrical characterization to understand the relationship between composition and electrical properties. To design new materials with desirable properties, it is crucial to have a comprehensive understanding of the relationships between the composition, structure, and properties of the material. This requires a deep understanding of the mechanisms involved in the formation and behavior of the material. Therefore, the study aims to provide a systematic understanding of the properties of sodium borophosphate glasses and their dependence on the amount of NaI in the composition.

5.2. Experimental

5.2.1 Materials used

Raw materials such as boric acid (H_3BO_3), ammonium dihydrogen phosphate ($ADP-NH_4H_2PO_4$), sodium bicarbonate (Na_2CO_3) and sodium iodide (NaI) were used for preparation of electrolyte materials.

5.2.2 Preparation method

The conventional process of melt quenching is employed for the preparation of glass electrolyte samples. The samples of ionic glass series were prepared initially by taking an adequate quantity of the chemicals and thoroughly mixing them within an agate mortar pestle. Following this, the mixture was kept in the preheated furnace (450℃) for two hours to eliminate NH_3 and CO_2 gas from it. Subsequently, the mixture was allowed to melt at temperatures ranging from $900℃-950℃$ for eight hours then being cooled between two pre-cooled copper blocks. For all glass compositions, the created glass specimens were nearly transparent. In order to eliminate any thermal stresses that may have been present in the glass as a result of rapid cooling (quenching), I had placed the glass samples in a furnace

at a temperature of 150℃ for a duration of half an hour. The Table 5.1 contains a list of the solid electrolyte samples that vary in the concentration of the additive halide-NaI while maintaining the equal ratio of glass former to the modifier.

5.3 Results and discussion

5.3.1 Physical Characterization

The Archimedes principle was used for density measurement of each glass sample (described in chapter 3, section 3.3.1). The molar volume V_m, oxygen packing density (OPD), oxygen molar volume V_o, cation concentration from modifier oxide N_{oxide} and iodide N_{iodide}, and the cations at the Fermi energy (E_f) level that will participate in the conduction process have been computed from the density and are listed in Table 5.1.

***Table 5.1**: Physical parameters of Sodium borophosphate (NBP) glass electrolyte system*

Sample code	Network former ($B_2O_3-P_2O_5$) (wt.%)	Network modifier (Na_2O) (wt.%)	Additive (NaI) (wt.%)	Density ρ (g/cc)	Molar volume V_m ($cc/mole$)	Oxygen Packing Density OPD ($mole/l$)	Oxygen Molar Volume V_o ($cc/mole$)	cation concentration N_{oxide} x 10^{21} /cc	cation concentration N_{iodide} x 10^{21} /cc	Total cation concentration N x 10^{21} /cc	N at E_f w.r.t total cation concentration(%)
NBP1	69.3	29.7	1	2.4888	52.2136	61.4322	16.2781	4.5680	0.1154	4.6833	28.59
NBP2.5	68.25	29.25	2.5	2.4818	52.3232	60.3746	16.5632	4.4893	0.2878	4.7771	28.93
NBP4	67.2	28.8	4	2.4790	52.5063	59.2385	16.8808	4.4049	0.4588	4.8637	29.17
NBP5	66.5	28.5	5	2.4739	52.6986	58.4075	17.1210	4.3431	0.5715	4.9145	28.79
NBP10	63	27	10	2.4790	52.2617	55.7960	17.9224	4.1489	1.1525	5.3014	28.58
NBP15	59.5	25.5	15	2.4959	53.0573	51.9061	19.2655	3.8596	1.7028	5.5624	28.37
NBP20	*56*	24	20	2.5017	53.3450	48.5893	20.5806	3.6130	2.2581	5.8711	27.95

The measured density values slightly decrease with the increase of NaI given in Table 5.1 and seen in Fig. 5.1 (a). The molar volume of the glass samples increases slightly up to

NBP5 with the addition of NaI and then decreases, which further starts increasing after NBP10 giving an anomaly in the mobility of cations [16]. The changes in oxygen packing density, oxygen molar volume, and cation concentration suggest that the addition of a modifier oxide (which causes the formation of NBOs) and NaI concentration have caused structural changes in the glass system. The decrease in oxygen packing density $61.4322\ (mole/l)$ to $48.5893\ (mole/l)$, suggests that the addition of the modifier oxide has caused the glass structure to open up, resulting in the formation of NBOs. The increase in oxygen molar volume from $16.2781\ (cc/mole)$ to $20.5806\ (cc/mole)$ further supports this conclusion, as it indicates that there is more space available for oxygen molecules in the glass system. The changes in cation concentration also suggest structural changes in the glass system. The decrease in N_{oxide} concentration and the increase in N_{iodide} concentration indicate that the total cation concentration has increased with the addition of NaI concentration from $4.6833\ x10^{21}/cc$ to $5.8711\ x10^{21}/cc$, Fig. 5.1 (b), in the glass system. The total cation concentration rises with increasing NaI concentration, as seen in Table 5.1. Since the additive halide releases more Na^+ ions than the modifier oxide. For a sample code, NBP4, which has been found to have the highest percentage of cation concentration at the Fermi energy level (Fig. 5.1 (c)). This observation suggests an increase in defect energy states or free charge carriers [17], which could result in an increase in the mobility of charge carriers with low activation energy for ion transport. This, in turn, can lead to an enhancement of the ionic conductivity of the glass sample.

5.3.2 Thermal Characterization

The FIC glasses are viewed as decoupled systems in which the motion of mobile ions is due to their decoupling from the rigid glass network [18]. The decoupling index of the glass system can be determined solely using the glass transition temperature. TGA scans were recorded from ambient temperature to 1000 ℃, to investigate the thermal behavior of the glass systems in terms of the glass transition temperature, as shown in the Fig. 5.2. It appears that the addition of salt to the material caused a decrease in T_g up to $4\ wt.\%$ of NaI salt, after which T_g increased linearly with increasing salt concentration. This suggests that the addition of salt affected the mobility of the molecules, of the material, in a non-linear way. At low salt concentrations, it seems that the addition of salt caused charge carriers to be liberated from the glass, which in turn caused the material to become softer and more mobile, leading to a decrease in T_g.

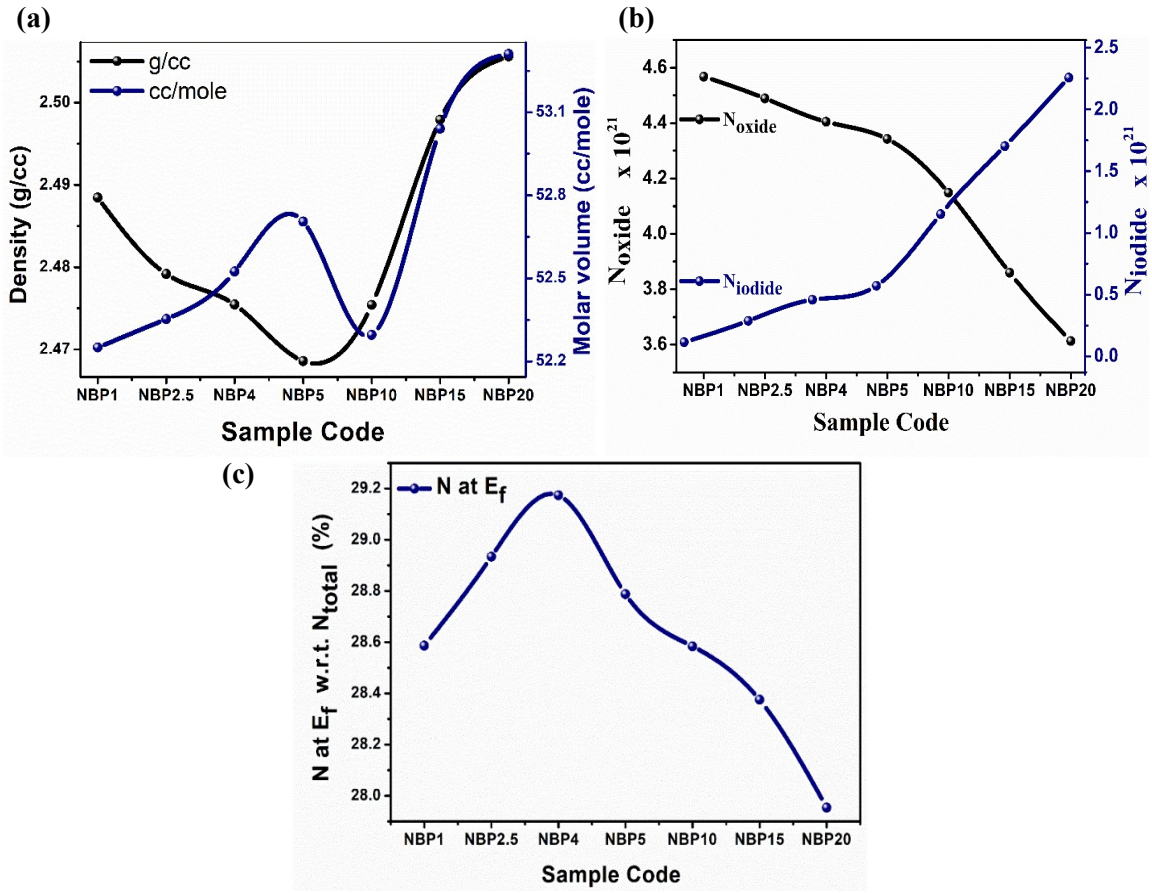

***Figure 5.1**: (a) Density and molar volume as a function of NaI additive concentration, (b) variation of number of charges as a function of glass composition, (c) cation concentration at Fermi energy level as a function of glass composition.*

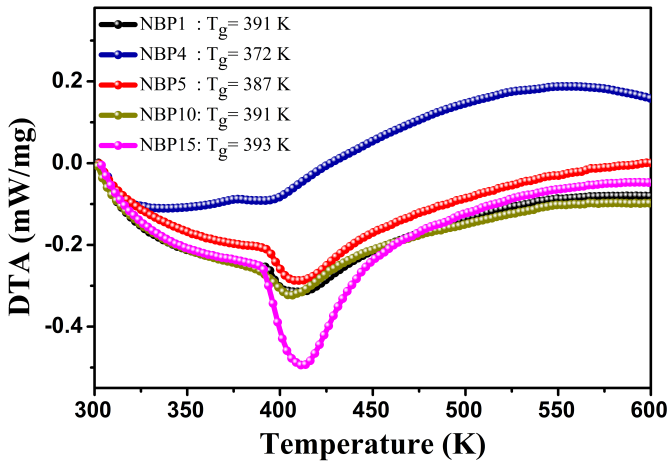

***Figure 5.2**: DTA thermographs for glass transition temperature of NBP glass system.*

However, at higher salt concentrations, the effect of the added salt on the material's mobility changed, causing the material to become stiffer and more ordered, which led to an increase in T_g [19].

5.3.3 Structural Characterization

a) X-ray Diffraction study

It is well-established in the literature that adding salt to a system can have an effect on the amorphosity of the system and enhance the mobility of ions. The X-ray diffraction profile of NBP series samples, as shown in Fig. 5.3, exhibits broad and diffused humps at around $30° - 50°$, which continuously widen with increasing salt concentration. This indicates that the full width at half maximum (FWHM) of peak increases with increasing salt concentration. The broadening of the XRD peaks is attributed to the increased disorder in the system due to the addition of salt. As the salt concentration increases, the ions become more mobile and disorder is introduced in the system, leading to a broadening of the diffraction peaks. This increased disorder is indicative of a higher degree of amorphousness in the system. It demonstrates that a study on the effect of salt concentration on the amorphosity and ionic conductivity of a prepared system.

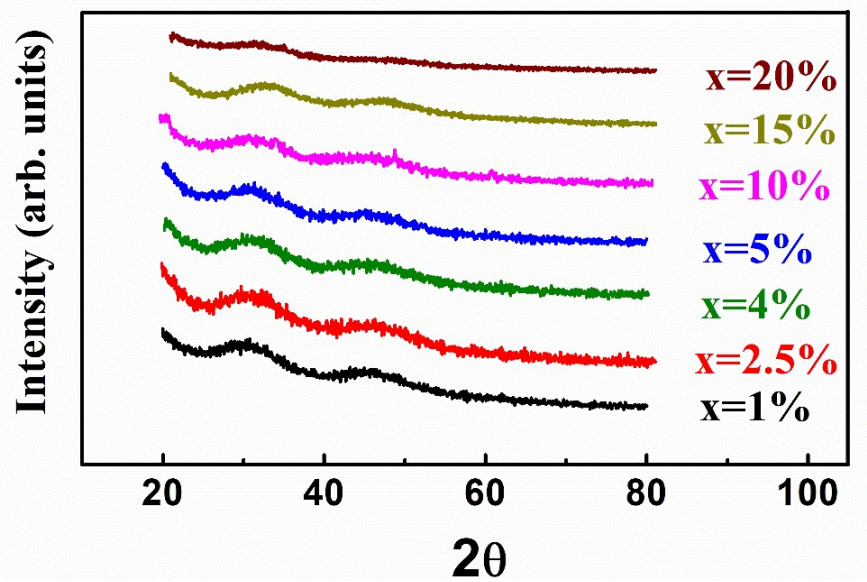

Figure 5.3: *X-ray diffraction pattern for NBP glass series compositions.*

As the salt concentration increases, the system becomes more amorphous, which is likely due to an increase in the mobility of the backbone structure. This, in turn, is expected to improve the ionic conductivity. However, there is a hump in intensity that reduces above a salt concentration of 4 $wt.\%$. The produced samples are entirely amorphous and glassy, as evidenced by the sharp peak-free XRD pattern, which indicates that no crystallization process has occurred. The non-crystallinity of the glass samples was also confirmed through thermal characterization.

b) Fourier Transform Infrared (FT-IR) Spectroscopy study

Infrared (IR) spectroscopy is a powerful technique used to study the vibrational properties of molecules. When a molecule absorbs infrared radiation, it undergoes a change in its vibrational energy, resulting in a characteristic absorption spectrum that is unique to that molecule. In glassy substances, the vibrational absorption bands are usually wider and more overlapped than in their crystalline counterparts. This is because of the random structure, with a dispersed distribution and a lack of long-range order. The IR transmission spectra depicted in Fig. 5.4 can provide important information about the vibrational properties of the glassy substances under study. The important peaks are also listed in Table 5.2. By analyzing the spectra, researchers can identify the various vibrational modes of the molecules within the glass and obtain information about their frequencies, intensities, and shapes. Changing the doping concentration while holding the modifier-to-former ratio constant can cause structural grouping rearrangements of vibrational spectra in the NBP glass series, which can be analyzed using Fourier transform infrared spectroscopy (FTIR). The resulting spectrum provides information about the vibrational modes of the sample, and changes in the spectrum can reveal changes in the molecular structure of the sample.

In the current system, the glass-forming compounds are B_2O_3 and P_2O_5. The examination of FTIR spectra revealed the presence of borate (BO_3, BO_4), phosphate (PO_3, PO_4), and borophosphate ($B-O-P$) structural units in the present glasses. When Na_2O incorporates into the matrix of borophosphate glass, it changes trigonal borate structural clusters to stable tetragonal borate units, while the phosphate chain depolymerizes and is also responsible for NBO formation. The incorporation of NaI halide additive in deformed borophosphate glass system can have different effects on ion migration, depending on the concentration and specific conditions of the system.

In general, the addition of NaI halide can enhance ion migration in borophosphate glass, especially for alkali ions such as sodium (Na^+). This is because the halide ions (I^-) can form ion pairs with the alkali ions, which reduces the effective charge of the alkali ions and lowers their activation energy for diffusion. Therefore, the addition of NaI can promote ion conduction and improve the ionic conductivity of the glass. However, at higher concentrations of NaI, the opposite effect can occur, where the ion migration is hindered instead of encouraged. This is due to the formation of NaI clusters, which can act as barriers to ion migration and impede the movement of ions through the glass matrix. Additionally,

the formation of these clusters can lead to phase separation and the formation of a less homogeneous glass structure, which further reduces the ionic conductivity.

The first band in the far-infrared region is seen at the 460 cm^{-1} band, whose intensity increases with increasing sodium iodide content, may be assigned to vibration due to cation motion [20]. $P-O-P$ bending peak at 530 cm^{-1}, does not show any observable change with the addition of NaI, while $B-O-B$ bending peak gradually shifts from 711 cm^{-1} to 684 cm^{-1} till 4 $wt.\%$ addition of NaI salt, suggestive of increases the bond length of a characteristic band. However, it remains unchanged at 706 cm^{-1} for $NBP5$, $NBP10$, $NBP15$ and $NBP20$ samples.

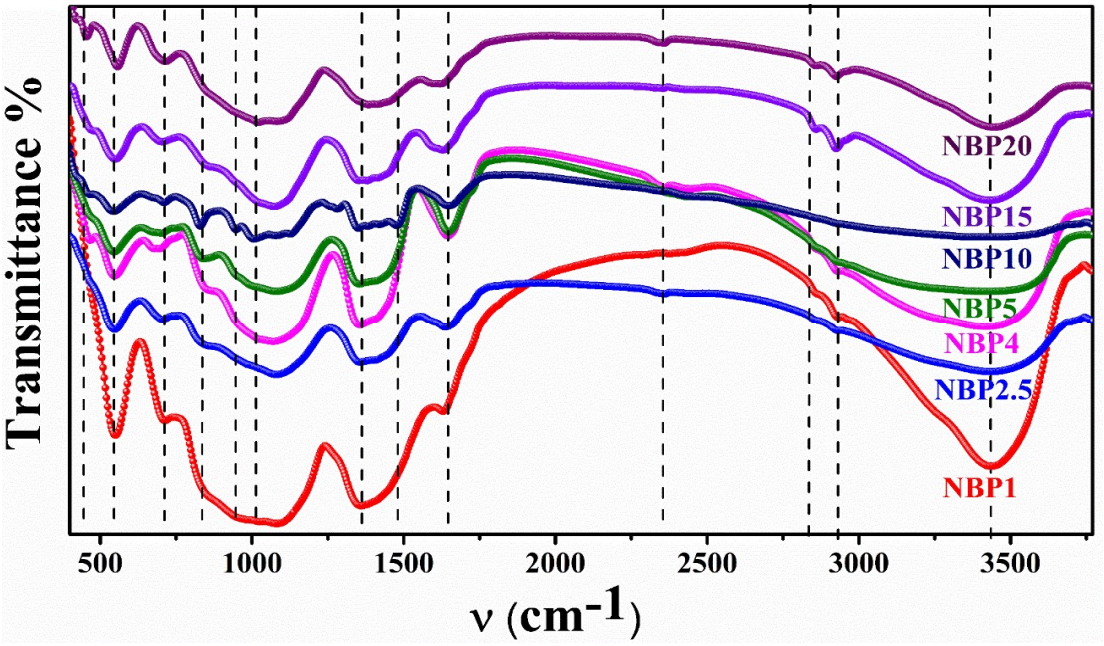

Figure 5.4: *FT-IR spectra of NBP glass compositions between* 400 cm^{-1} *to* 4000 cm^{-1} *wave number.*

It appears that the addition of NaI has an effect on the absorption peaks in the NBP samples. Initially, the NBP2.5 sample has a broad and less intense absorption peak, which evolves into a more intense peak at 850 cm^{-1} with further addition of NaI. The increase in intensity and shift in peak position to 850 cm^{-1} with NaI addition suggests that the boron-oxygen network is accommodating the larger size of the (I^-) anions by forming diborate clusters. This may be indicated by the relative strength of the absorption band at 850 cm^{-1}. However, beyond the NBP5 sample, the peak intensity of the $B-O$ bonds in BO_4 decreases and disappears altogether in the NBP20 sample. This could indicate that the boron-oxygen network is changing or breaking down, possibly due to the formation of new structures or compounds [21].

***Table 5.2**: Band positions and assignments of IR bands of present glass system.*

Wavenumber (cm^{-1})	Mode of Vibration	Assignment of IR band	Reference
~530	(δ_s)	• O=P-O bond due to deformation mode of PO- unit.	[22]–[24]
$684-720$	(δ_s) (ν_s)	• $B-O-B$ bridges of boron-oxygen network & $O_3B-O-BO_3$ linkage in various borate unit. • $P-O-P$ linkage bridge.	[14], [25]
$835-850$	(ν_s)	• $B-O$ bonds in BO_4 tetrahedra from diborate group.	[21], [26], [27]
~900	(ν_{as})	• The bridging $P-O-P$ groups.	[28]
$1130-1160$	(ν_{as})	• BO_3^- of penta borate unit.	[24], [29], [30]
$940-1080$	(ν_{as})	• $P-O-P$ bonds in PO_4^{3-} (ortho-chain like) and PO_3^- (meta-ring type) phosphate units.	[11], [31], [32]
$1080-1090$	(ν_s)	• $P-O^-$ bond structure.	[24], [28], [30]
~1102	(ν_s)	• $B-O$ bond of BO_4 tetrahedra units in various borate (di-, tri-, tetra-, penta-) rings.	[11], [17], [33]–[35]
$1130-1160$	(ν_{as})	• BO_3^- of penta borate unit.	[24], [29], [30]
~1250	(ν_{as})	• The cross-linked $B-O-P$ bond.	[17], [23], [25], [28], [29], [33], [36]
$1350-1370$	(ν_s)	• pyro- and ortho- borate groups of the BO_3 molecule.	[17], [33], [37]
~1630	(ν_{as})	• $B-O$ in trigonal BO_3 unit.	[17], [36]

Where, δ_s, ν_s and ν_{as} are the bending, symmetric stretching and asymmetric stretching mode of vibrations, respectively.

The observed pattern of variation in the intensity of infrared bands in $940-1080\ cm^{-1}$ region attributes to the asymmetric stretching mode of PO_4^{3-}. The depolymerization of the phosphate network is evident when the chain-like unit (PO_4^{3-}) transforms to the ring-type (PO_3^-) with the alkali halide salt amount. The band associated with the $P-O-P$ (ν_{as}) bond appears at a wavenumber of $935\ cm^{-1}$cm, and its strength increases up to $5\ wt.\%$ addition of NaI in the sample. In contrast, the absorption band for the $P-O-P$ (ν_s) bond is at a wavenumber of $700-750\ cm^{-1}$ with decreasing intensity [11], [38].

With $\geq 5\ wt.\%\ NaI$ addition, the phosphate groups restore from meta- to ortho- phosphate structural units and exhibit a lower intensity at $1078\ cm^{-1}$ wavenumber [39]. It seems likely that the electrostatic interactions between the positively charged Na^+ ions and the negatively charged phosphate groups occur due to the Coulombic attraction between opposite charges. This attraction can cause the Na^+ ions to bind to the phosphate groups, creating a bridge between adjacent chains. As more and more Na^+ ions bind to the chains, the cross-linking between them becomes stronger, leading to an increase in the strength of the overall structure [31]. Maximum peak intensity recorded at the wavenumber of

1056 cm^{-1}, identified for the symmetric stretching vibration of $B-O$ in BO_4 units, is with 4 $wt.\%$ halide salt doping. For the rest samples, their wavenumbers show the shifting to a higher side, and the intensity of the band recorded is low. The band at 1063– 1075 cm^{-1} is ascribed to the $B-O$ stretching vibration of the BO_4 units [20], it shows the broadened and intense band for the NaI addition up to 4 $wt.\%$ while the band shows flatness with the less intensity afterwards. The peak intensity for the absorption band the wavenumber $1080-1090\ cm^{-1}$ increases till $NBP4$ sample and after that it decreases and showing insignificant peak for $P-O^{-}$ symmetric stretching mode of vibration. In general, the bond between $P-O-P$ at $900cm^{-1}$ replace with $B-O-P$ bonds at 1250 cm^{-1}, resulting in an increase in the T_g and a highly cross-linked structure in the borophosphate glasses (on formation of tetrahedral BPO_4 units) [28]. Through $B-O-P$ linkages, structural networks are becoming more interconnected and show an effect on the T_g value. On the other hand, at 1250 cm^{-1} wavenumber, the higher intensity of the $B-O-P$ bond leads to a highly cross-linked structure, while the band for the $P-O-P$ bond is less intense, which altogether changes the ion conductivity and the glass transition temperature [28], [32], [40]. The wavenumber at 1258 cm^{-1} begins to evolve from the NBP5 sample, which displays strong interactions between the two network formers, boron oxide and phosphorus oxide, leading to the predominance of $B-O-P$ connections. Increased network phosphorous polymerization correlates with a considerable rise in glass transition temperature [41]. The peak between $1350-1370\ cm^{-1}$ corresponds to the symmetric stretching of the pyro- and ortho- borate groups of the BO_3 molecule, which shifts abruptly at 1340 cm^{-1} for the $NBP4$ sample, increases the pyro- and ortho-borate bond lengths of the borate group correspondingly, which is consistent with the results of the thermal investigation. The trigonal BO_3 unit exhibits a distinctive band at the wavenumber 1630 cm^{-1} for $x=1, 2.5,$ and 4 $wt.\%\ NaI$ in the studied glass system. It transits to a higher wavenumber with a more intense peak for the remaining samples, indicating the structural changes in trigonal borate by the $B-O$ bond of BO_3 units [36], and so does the rigidity of a structure. At 1076 cm^{-1}, the broadband is seen in NBP which corresponds to the vibration of stretching of $B-O-B$ bond of tetra-borate groups of BO_4 [42]. The structure of oxide glasses, such as borophosphate glasses, is dependent on the packing of the glass network. The cross-linking of the network in borophosphate glasses can lead to an increase in the glass transition temperature, which is a measure of the thermal stability of a glass. The presence of mixed glass-formers can also contribute to the thermal stability of

the glass network. Therefore, changes in the composition of the glass can affect the glass transition temperature, making it an important parameter to consider when designing new glass compositions with specific properties [8]. It is true that the presence of multiple glass-forming oxides in a network can increase the number of structural units in a glass, which can lead to the emergence of new vibrational bands in the infrared spectra of the material. In the case of borophosphate glasses, the addition of borate and phosphate units to the basic borophosphate network can result in the formation of new structural units that exhibit distinct vibrational modes in the infrared spectra. Researchers have indeed studied the infrared spectra of borophosphate glasses and have identified the presence of new borate, borophosphate, and phosphate units in the network. These units can connect to the existing borate groups in the network and form new structural motifs that contribute to the overall vibrational spectrum of the material. The identification of these new structural units and their vibrational modes can provide valuable insights into the atomic-scale structure of borophosphate glasses and can help researchers understand the factors that govern their properties, such as mechanical strength, thermal stability, and chemical durability [8]. In the examined system, the FTIR spectra of all samples exhibit dominant BO_3 structures centered at 1355 cm^{-1} and 700 cm^{-1}. For low amount of salt, the peak shifts to lower wavenumbers and shows that the BO_4 structural units predominate, which is explained by the high peak intensity at wavenumbers about 1055 cm^{-1} and 949 cm^{-1}. FTIR spectra of the present study conclude that the following are the primary bonds which play a crucial role in comprehending the effect of NaI addition to the sodium borophosphate glass system. (i) Borate (trigonal and tetragonal) unit: The FTIR spectra show changes in the vibrational modes of the borate units, indicating changes in the borate network structure upon the addition of NaI. The frequency and intensity of the characteristic borate bands are altered, indicating the breaking and formation of borate bonds in the glass structure. (ii) Phosphate (poly and depolymerized) unit: The vibrational modes of the phosphate units, indicates that the addition of NaI affects the phosphate network structure pointing out the breaking and formation of phosphate bonds in the glass structure. (iii) $P-O-P$ and $B-O-P$ bond formation and show changes in the intensity and frequency of $P-O-P$ and $B-O-P$ bands, indicating the formation and transformation of these bonds in the glass structure. The changes in these bands suggest the reorganization of the glass network due to the addition of NaI.

5.3.4 Electrical Characterization / Impedance Spectroscopy

The impedance spectra of the NBP glass series electro material, depicted in Fig. 5.5(a-g), were studied using the impedance formalism technique. It illustrates the effect of increasing amounts of NaI on the impedance response of the host glass system, $Na_2O - B_2O_3 - P_2O_5$. The impedance plots for all NBP series compositions over the temperature range of 303 K to 410 K, the complex impedance spectra of glasses were measured using the Solartron-1260A for the frequency range of 1 Hz to 32 MHz. As seen in impedance spectra, a small semicircle appears in the high-frequency regime, because of net ion displacement and the relaxation of mobile ions (long-range ion migration), which occurs before ions accumulate at the electrode-electrolyte interface. However, a larger semicircle in the lower-frequency region of the impedance spectrum is likely due to the presence of this immobile layer of ions, which creates a kind of "barrier" to the flow of current in the material. As the frequency of the electric field increases, this barrier becomes less effective, and the impedance decreases accordingly [43]. The semi-circular arc represents bulk conduction, while the spur results from the polarization of the electrode. In the studied frequency range, it is noticed from Fig. 5.5(f) that the appearance of the spike in the high-temperature zone is consistent with ion mobility being thermally stimulated [44]. Nyquist plot and the equivalent circuit for the NBP glass sample at different temperatures wherein the bulk resistance of the specimen (R_b) is determined using the intercept of an arc with the real axis (Z').

a) DC conductivity

The knowledge of the physical dimensions of the test samples and the value of bulk resistance (R_b) from the Nyquist plot allow to determine the dc conductivity of the material using Eq. (5.1).

$$\sigma_{dc} = \frac{t}{R_b A} \quad \ldots\ldots (5.1)$$

Where, σ_{dc} is the dc conductivity, t is the thickness and A is the cross section area of the test sample. In the case of Nyquist plots with two semicircles, as shown in Fig. 5.5(a-g), the bulk resistance of the electrolyte is given by the diameter of the semicircle at a higher frequency. The higher-frequency semicircle is typically associated with a kinetically controlled charge transfer mechanism, such as a redox reaction at the electrode surface. The diameter of this semicircle provides information about the rate of the charge transfer reaction, as well as the resistance associated with the electrolyte solution.

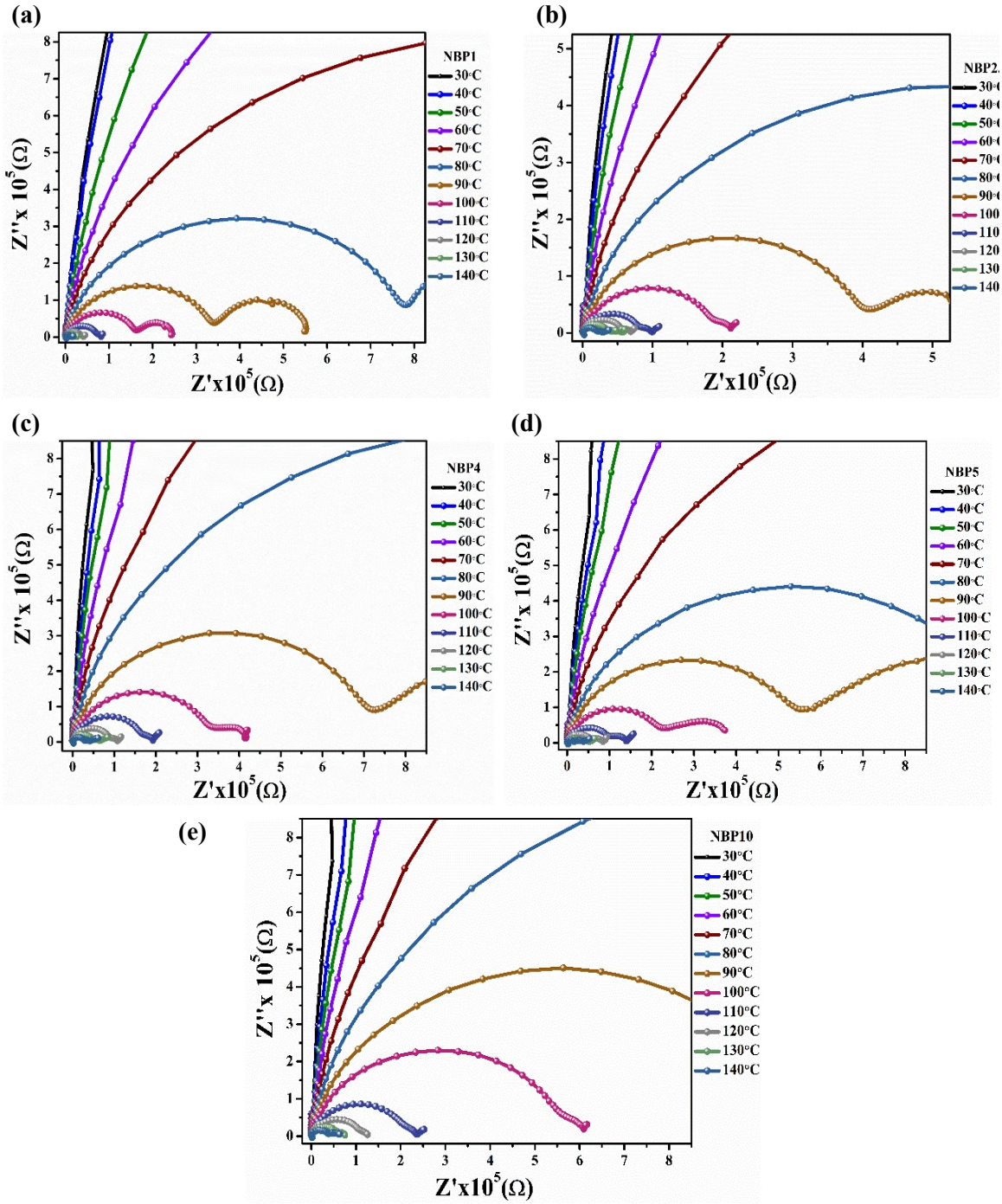

***Figure 5.5**: (a-e) Nyquist plots for NBP series samples for* $1, 2.5, 4, 5$ *and* $10\ wt.\%$ *of NaI addition in the sodium Boro-phosphate glass system.*

The larger the diameter of the semicircle, the slower the rate of the charge transfer reaction, and the higher the resistance of the electrolyte. The lower-frequency semicircle, on the other hand, is typically associated with the ion diffusion or "mass transfer resistance" of the electrolyte. This semicircle provides information about the transport of ions within the electrolyte solution, and the resistance associated with this transport. The size of the semicircle is related to the diffusion coefficient of the ions in the electrolyte, as well as the distance between the electrode and the electrolyte.

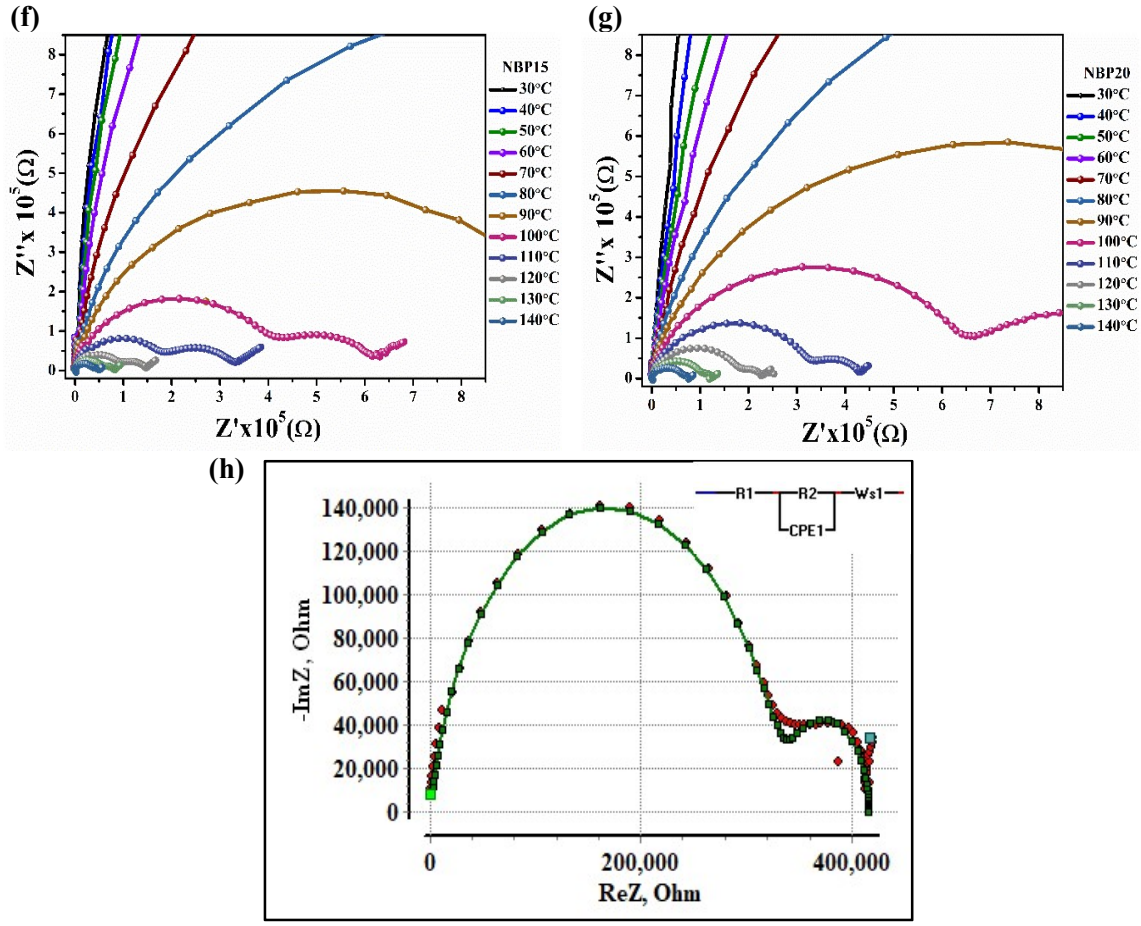

***Figure 5.5**:(f-g) Nyquist plots for NBP series samples for* 15 *and* 20 *wt.% NaI addition in the sodium Boro-phosphate glass system respectively, (h) Nyquist plot fitting with the equivalent circuit for NBP4 sample at* 373 *K temperature, inset: the model circuit elements (red points are the original data and green line is the fit result- guide to eyes).*

In addition to the ion diffusion, the lower-frequency semicircle can also be influenced by the interface between the electrode and the electrolyte. This interface can introduce additional resistance to the electrochemical system, particularly if it is not well-defined or if there is a large interfacial area between the electrode and the electrolyte [45]. To better comprehend electrochemical impedance spectroscopy profiles, an equivalent circuit model was used to fit Nyquist plots. When a Nyquist plot exhibits two semicircular arcs, it is often due to a series combination of two parallel lumped components, one being a resistor (R) and the other being a Constant Phase Element (CPE) as depicted in Fig. 5.5(h). The two semicircles in the Nyquist plot are associated with different relaxation times or time constants, which can provide information about the different processes occurring in the system. The high-frequency semicircle corresponds to a shorter relaxation time and represents the behavior of the system at higher frequencies. The low-frequency semicircle corresponds to a longer relaxation time and represents the behavior of the system at lower

frequencies. By fitting an equivalent circuit model to the Nyquist plot, it is possible to extract quantitative information about the system, such as the values of the resistance and capacitance components, as well as the time constants associated with the relaxation processes. The CPE element in an equivalent circuit (inset of Fig. 5.5(h)) signifies the distribution of glass properties, representing the electrode-electrolyte interface and known as double-layer capacitance effects (CDL). It can be seen from the Nyquist plots (refer Fig. 5.5(a-g)) that the arc at high frequency decreases in diameter and tends to move toward the origin of the graph, which indicates a decrease in overall impedance value with rising temperature. These temperature-related fluctuations are seen for other glass compositions as well. It is seen from the complex plots that the semi-circle in the higher frequency is larger than the low-frequency arc. The larger and smaller semi-circles evolved with the variation in the respective frequency regimes, according to the glass compositions depicted in Fig. 5.5(a-g).

Glasses are isotropic solids with negligible magnitudes of grain boundary resistance and capacitance [46]. The grain size of super ion-conducting glassy materials does not have an impact on their bulk conductivity. This finding was reported by Satyanarayan et al; [47] in a previous publication. The impedance semicircles obtained from the materials exhibit a center below the real axis of the complex plot. The presence of an asymmetry between the electrode and electrolyte interfaces may be responsible for this deviation. The angle between the complex plane origin and the center of the semicircle is around (~ 20 °). The slope of the low-frequency spike in the impedance plot also indicates the presence of distortion or deviation, possibly due to the aforementioned asymmetry. Additionally, the introduction of sodium salt of $20\ wt.\%$ in the glass composition leads to the manifestation of a polarization spike at high temperatures (Fig. 5.5(g)).

Fig. 5.6(a) demonstrates the temperature-dependent change in ionic conductivities. It is the curve of $\log \sigma_{dc}$ vs $1000/T$ for various NaI concentrations in system compositions. In accordance with Arrhenius (fitting) type behavior the conductivity of all samples increases linearly in a plot of $\log \sigma_{dc}$ vs $1000/T$.

$$\sigma_{dc}(T) = \sigma_0\ exp\left(\frac{-E_a}{kT}\right) \quad \ldots\ldots (5.2)$$

Where σ_{dc} is the ionic conductivity of direct current, T is the temperature in Kelvin, E_a is the activation energy of Na^+ ions, and σ_0 is the pre exponential factor or say ionic conductivity at $0\ K$ temperature.

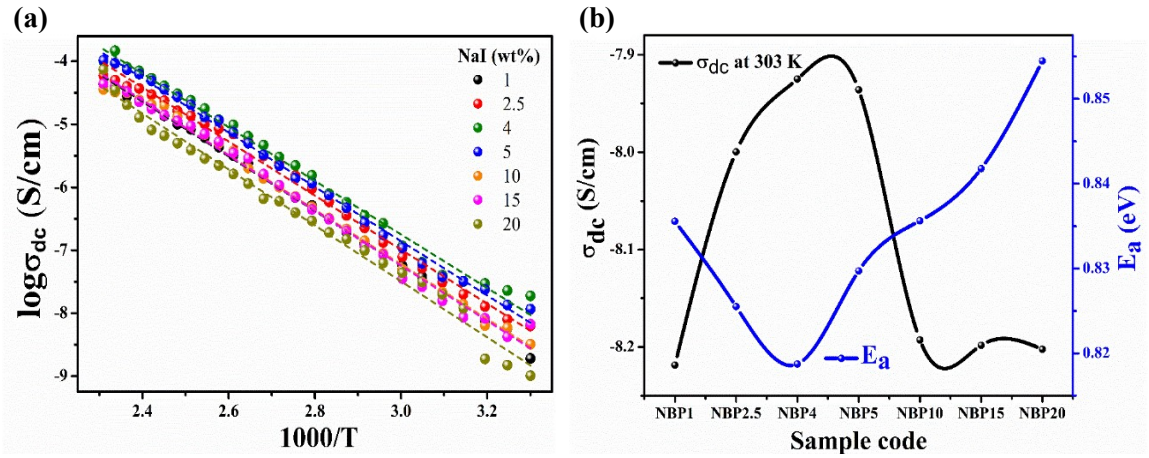

***Figure 5.6**:(a) Variation of R_τ with temperature as a function of compositions of NBP glass series. (b) Variation of dc conductivity (σ_{dc}) and its corresponding activation energy (E_a) for NBP series samples.*

The activation energy necessary for the migration of Na^+ ions in the glassy matrix was calculated by fitting dc conductivity graphs with the Arrhenius equation, as shown in Eq. (5.2). Fig. 5.6(b) displays the activation energy and room temperature conductivity of the glass system. The value of σ_{dc} consistently rises with sodium iodide content, peaking at $1.18883x\ 10^{-8}\ S/cm$ for $x = 4\ wt.\%$ of the NaI concentration. While the E_a value, which is activation energy follows the reverse trend as expected. The activation energy (E_a) follows a countertrend to the ionic conductivity, as expected from Eq. (5.2). For the studied system, the activation energy is $80.62364\ kJ/mole$ at $x = 1\ wt.\%\ NaI$, which drops to $78.99935\ kJ/mole$ at $x = 4\%$ and then increases from $x = 5\ to\ x = 20\ wt.\%$ of NaI and peaks at the highest value of $82.44797\ kJ/mole$ at x=20% of NaI. Another way to obtain dc conductivity is by using the frequency-independent plateau portion of the conductivity spectrum (discussed in the next section).

The Weak Electrolyte Model is a model used to explain the behavior of weak electrolytes, which are substances that only partially dissociate into ions in solution. This model predicts that the concentration of stoichiometric ions, which are the ions predicted by the balanced chemical equation of the electrolyte, will be higher than the effective concentration of cations, such as sodium ions (Na^+), due to the ion-pairing phenomenon. The conductivity and activation energy variations in the system under investigation can be explained by this model, as the effective concentration of cations will affect the ion transport and conductivity of the solution. In addition, the Ravaine-Souquet (R-S) model can be used to understand the transport phenomenon in weak electrolytes, as it considers the effects of ion pairing and dissociation on ion transport. With increasing NaI concentration in the studied system, the

total number of cations according to stoichiometry will rise, as more NaI molecules will dissociate into their constituent ions in solution. However, the effective concentration of cations may not increase proportionally, as some of the ions may form ion pairs with counter ions, leading to a decrease in the mobility of the ions and the conductivity of the glass. However, the number of cations present at E_f (for conduction) is less than expected based on stoichiometry. The data in Table 5.3 displays the Na^+ cation concentration as determined by the stoichiometric calculation and the interpretation of experimental data. According to the R-S model, two kinds of carrier ion populations, "mobile" and "immobile," are assumed to be present. The measured activation energy E_a is the quanta of energy needed to convert a population of immobile ions into a mobile state [48].

In our study, the NaI amount increases the conductivity (peak at $x = 4\ wt.\%$) of sodium boro-phosphate glasses. The higher conductivity causes due to either the Na^+ charge carriers or the carrier mobility according to Eq. (5.3).

$$\sigma_{dc} = constant\ [Na^+] \quad \ldots\ldots (5.3), \qquad and\ \mu = \frac{\sigma_{dc}}{[Na^+]\, z\, e} \quad \ldots\ldots \quad (5.4)$$

The constant is defined by the Eq. (5.4) which is in terms mobility, atomic number and the charge of the carrier. Where, μ is the mobility of charge carriers ($m^2V^{-1}s^{-1}$), $[Na^+]$ is the cation concentration ($atoms/cc$), z is the atomic number and e is the charge on carrier. Isard et al; have proposed the assumptions that the mobility of the Na^+ ion is unaffected by the composition and structure of the glass and defined the energy of activation, as expressed by Eq. (5.5). Since ionic conductivity is a result of equilibrium, it is not dependent on the thermodynamic activities of the alkali oxide [49], [50].

$$E_a = \frac{\Delta H}{2} + E_m \ldots\ldots (5.5)$$

Where E_a is the energy quanta for ion conduction, ΔH is the dissociation enthalpy and E_m is the true migration barrier, (all the energies are in eV).

Fig. 5.7(a) shows the percentage of cation concentration at the Fermi energy (E_f) level and mobility of them for all the prepared samples of the present glass system. While, Fig. 5.7(b) is the amount of Na^+ ions in all the materials increases until $x = 20\ wt.\%$ of NaI, seen from the plot. The charge carrier density as well as their mobility at (E_f) level are highest in sample NBP4, though. The simple explanation for conductivity reduction in the studied system was based on the assumption that all alkali ions were equally mobile.

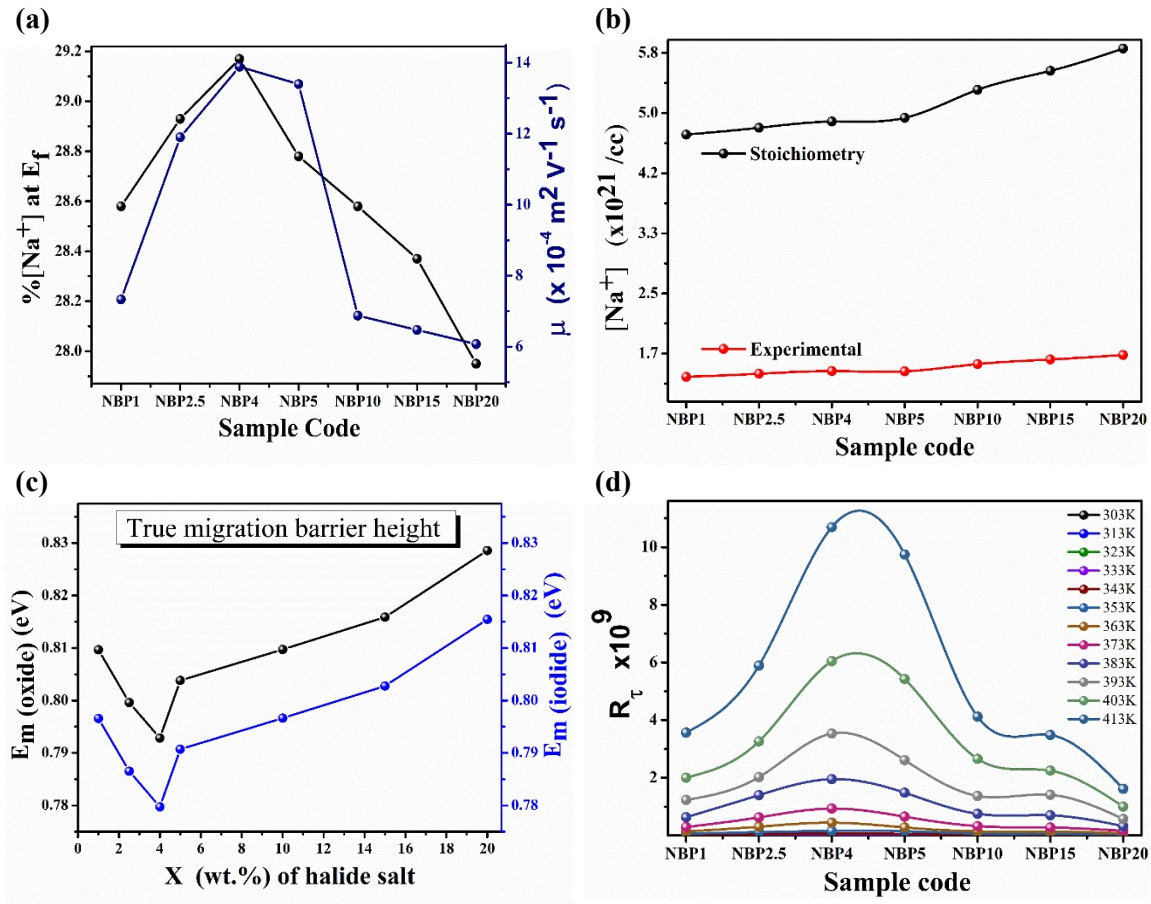

***Figure 5.7**: As a function of NBP glass compositions, (a) % of Na^+ ions at Fermi energy level and mobility of carrier ions, (b) Concentration of Na^+ ions calculated using empirical equation and from the experimental analysis, (c) The true migration barrier height for sodium oxide and iodide compound as a function of iodide salt, and (d) Decoupling Index profile for various temperatures for NBP series samples.*

However, the observed variations in the direct current conductivity (σ_{dc}) are not solely due to the concentration of charge carriers, but rather due to ion mobility and the net number of charge carriers having energy equivalent to the Fermi energy [51]. The strong electrolyte/cationic interaction paradigm assumes that in a solution or a solid electrolyte, the mobile ions are primarily responsible for electrical conduction. The variations in conductivity are due to two factors: ion mobility and the net number of charge carriers having energy equivalent to the Fermi energy. Ion mobility refers to the ability of ions to move in response to an applied electric field. The statement suggests that not all alkali ions have the same mobility, which contributes to the observed variations in conductivity. The net number of charge carriers having energy equivalent to the Fermi energy refers to the number of ions in the system that have energy levels equivalent to the Fermi energy, which is a measure of the energy required for an ion to move freely in the system. Martin and Christensen noted that the novel interpretation of Na^+ ion conduction in the mixed glass

former is that, according to the 'Weak Electrolyte' theory, only dissociated/decoupled ions give rise to conduction. Dissociation makes conduction more efficient by making mobile carriers available for conduction [52], [53]. Observed in Fig. 5.7(b) is that, consistent with stoichiometry, the experimental data show that the cation concentration rises with NaI. Ions in a solid can be mobile and conductive only when they are dissociated from the crystal lattice and free to move. This dissociation process requires energy, which is known as dissociation enthalpy. Until this energy is supplied to the system, the ions will remain immobile and unable to conduct electricity. In addition to the dissociation enthalpy, there is also a true barrier height that must be considered in the conduction process. The true barrier height represents the energy required for an ion to move from one site to another in the solid lattice. This energy barrier is the result of the interactions between the ion and the lattice, such as the electrostatic forces and the structural constraints of the lattice. The relationship between the activation energy and the true barrier height is important because it provides insight into the nature of the conduction process. This energy is related to the true barrier height, which represents the energy required to reach the transition state between two lattice sites, shown by Fig. 5.7(c).

Table 5.3*: The characteristics parameter of conductivity and its derivatives.*

Sample Code	Activation energy E_a (eV)	Calculated at 303 K		Cation concentration $[Na^+]$ $x\ 10^{21}$ $/cc$		$\%[Na^+]$ at E_f	Charge carrier mobility $\mu\ x\ 10^{-4}(m^2V^{-1}s^{-1})$	True migration barrier height (eV)	
		Conductivity $\sigma_{dc} x\ 10^{-9}\ (S\ cm^{-1})$	Decoupling index $R_r\ x\ 10^6$	Stoichiometry	Experimental			$E_{m\ (oxide)}$	$E_{m\ (iodide)}$
NBP1	0.8355	6.04	1.20	4.6833	1.3387	28.58	7.33	0.8096	0.7965
NBP2.5	0.8255	10.00	1.99	4.7771	1.3822	28.93	11.90	0.7996	0.7865
NBP4	0.8187	11.88	2.37	4.863	1.4189	29.17	13.88	0.7928	0.7797
NBP5	0.8297	11.58	2.31	4.9145	1.4147	28.78	13.39	0.8038	0.7907
NBP10	0.8356	6.41	1.28	5.3013	1.5153	28.58	6.87	0.8097	0.7966
NBP15	0.8417	6.33	1.26	5.5624	1.5783	28.37	6.47	0.8158	0.8027
NBP20	0.8544	6.27	1.25	5.8711	1.6411	27.95	6.07	0.8285	0.8154

In the present investigation, the sample NBP4 has a low effective barrier height, indicating low activation energy and a high concentration of dissociated (decoupled) ions possessing the energy equivalent to Fermi Energy (E_f) (refer Fig. 5.1(c)). By referring to a scientific

or technical articles, Fig. 5.7(d) and Table 5.3 are describing the behavior of certain glass compositions with varying NaI salt content. In an ion conducting glass system, the decoupling index, R_τ, measures how strongly mobile ions are getting decoupled from the glass matrix [24], [54], and practically it is explained by the ratio between the average relaxation times of the structural (τ_s) and the conductivity (τ_c) mechanism. Fig. 5.7(d) shows that the R_τ values increase steadily with increasing NaI content up to $4\,wt.\%$ sodium salt in the glass composition. The increase in the decoupling index ($x\ wt.\%$) shows that the structural changes in glass offer a low migration barrier and supports a high concentration of free mobile cations with Fermi-level equivalent energy. The characteristic conductivity parameter and its derivatives are listed in Table 5.3 for the NBP series samples by considering the $x\ wt.\%$ variation of NaI salt.

b) Frequency dependent conductivity

One way to study the ion transport phenomena is by analyzing the impedance spectrum. Impedance spectroscopy measures the electrical response of a material to an applied alternating current over a range of frequencies. By analyzing the impedance spectrum, one can extract information about the ion transport behavior in the material, such as the ion concentration, mobility, and diffusion coefficient. The theoretical explanation of the frequency-dependent conductivity in terms of the distribution of ion migration through hopping probabilities between randomly dispersed energy sites was first proposed by Pollak and Geballe [55]. This model assumes that the ions hop between localized energy states with different energies, and the probability of hopping between these states depends on the energy difference and the distance between the states. The frequency dependence of electrical conductivity in solid electrolytes as the result of the distribution of relaxation times was typically studied by Jonscher [56] and Ngai [57]. This model assumes that the relaxation process of the ions is non-exponential, and the relaxation time distribution is broad. The non-exponential relaxation can be attributed to the presence of multiple relaxation mechanisms, such as ion hopping, ion diffusion, and electrode polarization.

The proposed idea of Jonscher [56], who suggested that dispersion is a universal property of dielectric materials, was supported by the microscopic theories by Ngai [57], Dissado and Hill [58], wherein they demonstrated that dispersion is an inevitable consequence of dominating many-body interactions between charge carrier species. The coulombian interactions between the charge carrier particles are correlated to the phenomenon called "Hopping", in which the mobility of charge carriers is greatly influenced by surrounding

(local) relaxation events. The charge carriers (cations) occupy energetically favorable locations associated with negatively charged atoms in the material. They can hop from their initial site to the neighboring site in a process that satisfies the equilibrium condition. However, if a charge carrier fails to jump consistently, the screening effect caused by the charge carrier affects the other charge carriers and results in a non-equilibrium situation. This leads to a slow relaxation process of the local environment, which can result in a correlated sequence of forward and backward hopping. If the backward jump does not occur before the screening charge relaxation is completed, the hop is successful and results in diffusion. At low frequencies, only successful hops contribute to the conductivity, resulting in a constant value at dc (plateau region).

However, at higher frequencies, unsuccessful jumps contribute to the dispersive conductivity, which changes the conductivity trend from a constant value at low frequency to a power law dependent behavior. This mechanism of charge carrier diffusion in disordered materials has important implications for the electrical properties of glasses and other disordered materials. Fig. 5.8(a-g) displays the frequency-dependent conductivity spectra obtained for the $xNaI$ doped glass composition under study at various temperatures ($x = 1, 2.5, 4, 5, 10, 15,$ and $20\ wt.\%$). It is seen from the plots that the conductivity improves as the temperature rises. The conductivity spectrum exhibits two regions (i) a dispersion region at high frequency, and (ii) a frequency-independent plateau region corresponding to dc conductivity at low frequency. Fig. 5.8(h) displays the conductivity versus the log of frequency curve for all compositions of the glass system for the temperature of $373\ K$. Conductivity gradually improves as NaI weight percentage rises to the $4\ wt.\%$ iodide salt addition. The $NBP4$ sample exhibits the highest conductivity may be due to electrode effects and is usually seen in highly conducting substances [59].

In the studied frequency range, due to the high resistivity of the sample, nearly low-frequency dispersion is unable to see for $x = 5, 10, 15,$ and $20\ wt.\%$ of dopant content. However, for $x = 1, 2.5\ wt.\%$ of NaI, a hazy picture of low-frequency dispersion is exhibited. Electrode polarization is a phenomenon in which a voltage is applied across an electrode-electrolyte interface, charges begin to accumulate at the interface due to the movement of ions in the electrolyte solution. These charges create an electric field that opposes the applied voltage and can limit the current flow through the interface. This is known as electrode polarization indicated by the low-frequency dispersion observed in Fig. 5.8(a-h).

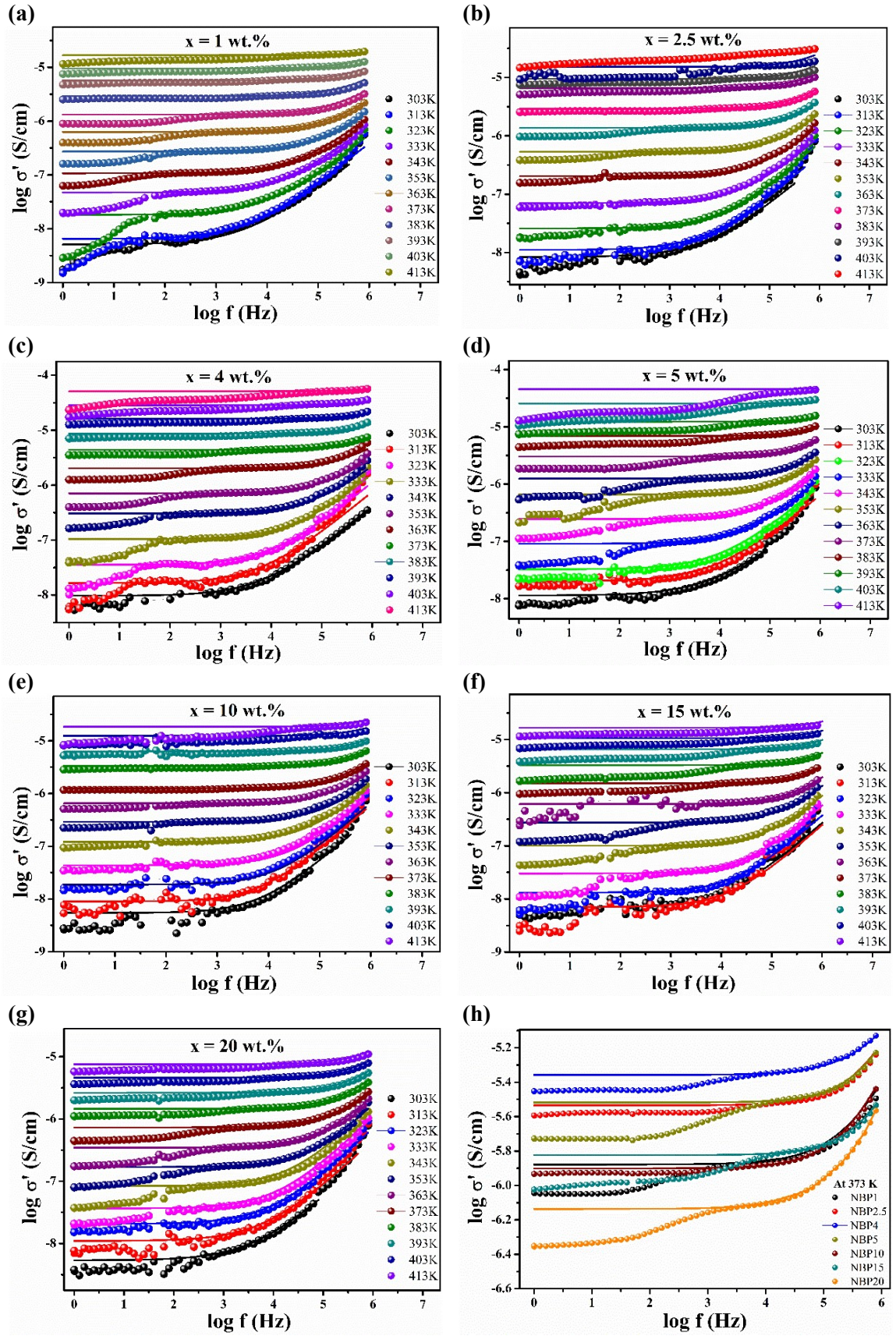

***Figure 5.8**:(a-g)The plots of σ′ vs frequency at various temperatures for $x = 1, 2.5, 4, 5, 10, 15, 20$ wt.%, respectively, (h) The plots of σ′vs frequency at 373 K for all the glass compositions (straight line represents the JPL fitting and guide to eyes).*

The electrode polarization can occur when the time intervals available to mobile ions at frequencies below $10\,kHz$ are sufficiently long that they can perform successful translational hops to nearby sites. The low-frequency plateau region observed in the dispersion plots indicates that the electrode polarization effect is dominant in this frequency range. As the frequency increases, the time intervals available for ion movement become shorter, which causes the low-frequency plateau region to shift towards higher frequencies [60], [61]. From Fig. 5.8(c), the polarization behaviour is observable and follows a plateau and high-frequency dispersion regions afterwards. The power law variation observed in these compositions has been extensively studied, and a significant dispersive trend at low temperatures in the high-frequency region is associated with the influence of many-body interactions [46].

In the studied system, the electrical conductivity is influenced by the motion of charged particles (such as electrons or ions) within the material. At low temperatures, the movement of these particles is limited, resulting in a lower electrical conductivity. As the temperature increases, the particles gain more thermal energy and move more freely, leading to an increase in conductivity. The frequency dependence of the electrical properties can also change with temperature. At low temperatures, the conductivity may be dominated by low-frequency processes, such as the hopping of charges between localized states. As the temperature increases, the charges can overcome larger energy barriers and start to move more freely, leading to a shift in the dominant frequency range towards higher frequencies. The jump frequency of charge carriers, as described by Ingram [62], is likely related to the rate at which charges move between localized states.

As the temperature increases, the charges are more likely to overcome energy barriers and jump between states, leading to an increase in the jump frequency. The power law exponent has been used to analyse the fluctuation in conductivity with frequency.

$$\sigma_{ac} = \sigma_{dc} + A(\omega)^n \ldots\ldots (5.6)$$

Where, $\sigma_{ac} = \sigma_{(\omega)}$ is the ac conductivity, σ_{dc}=σ_0 is the dc conductivity at zero frequency,ω is the radial frequency, A is the characteristic parameter, and n is the parameter dependent on temperature and frequency.

The power law of ac conductivity has been observed in many systems. Jonscher referred to this phenomenon as "Universal Behavior", also known as Jonscher power law (JPL). Since the power law Eq. (5.6) is accepted universally for determining the sample conductivity, hopping rate, and frequency dependence of conductivity.

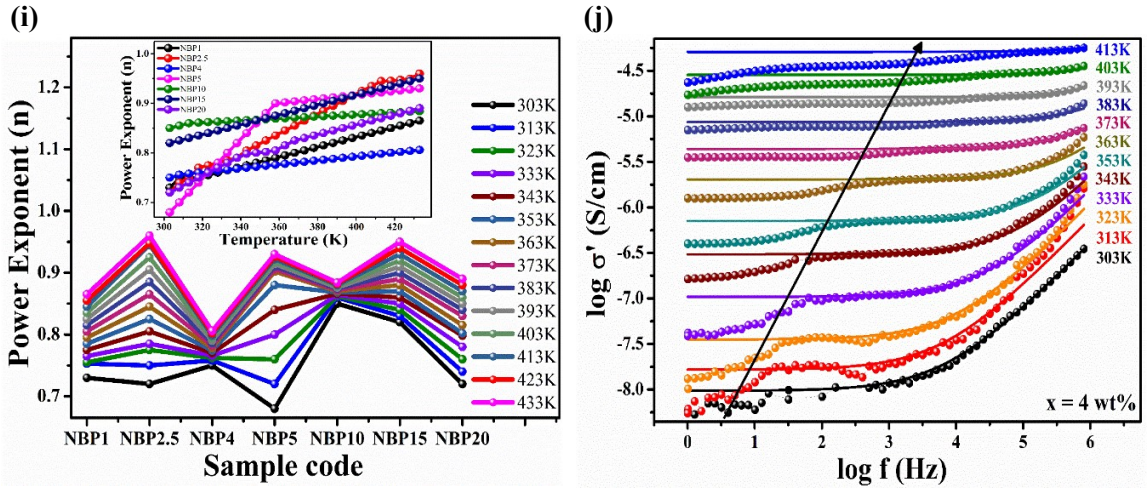

Figure 5.8 *:(i) Power law exponent* (n) *as a function of glass composition (inset: the behavior of* $n(T)$ *for all glass compositions), (j) The plot of* σ' *vs frequency for NBP4 sample at various temperature, the arrow show the hopping frequency (*ω_p*: changeover),*$\omega < \omega_p$ *lower frequency and* $\omega > \omega_p$*-higher frequency.*

From the investigation, the values of σ_{dc}, A, and n parameters have been acquired by fitting experimental data of frequency-dependent conductivity (σ_{ac}) at different temperatures. The characteristic parameter A increases with temperature, while the power law exponent $n(T)$ increases with temperature and demonstrates a value between $0.67 - 0.95$. Jonscher has demonstrated that a non-zero value of $'n'$ in the dispersive region of conductivity results from the storage of energy during short-range collective carrier motion [63]. A higher value of $'n'$ indicates that the cooperative carrier motion stores more energy. To comprehend the interaction between the ion and the network, frequency, exponent (n), has been discussed.

In the current system, $n(T)$ increases as the temperature increases depicted in Fig. 5.8(i). However, the $NBP4$ sample shows the lowest value of power exponent (at ≥ 323K, shown in inset of Fig. 5.8(i)), indicating a higher degree of modification in the network [24], [64], [65]. In the current system, analysis of the power exponent $n(T)$ confirms the hopping mechanism involved in conductivity [66]. The value of $n(T)$ explains the mechanism of conduction when the system is under the influence of an alternating current field. In the temperature range studied, $n(T)$ rises, which may attribute to the Non-Overlapping Small Polaron Tunnelling (NSPT) Model [64], [67]. According to NSPT model, at lower frequencies, a simultaneous decrease in $\sigma(\omega)$ is most likely caused by charge carrier polarisation at the electrode-electrolyte interface, followed by charge accumulation. Nearly frequency-independent conductivity is observed in the lower frequency regions $(\omega < \omega_p)$, where the ion successfully hops to nearby unoccupied sites, resulting in dc conductivity

[24]. The conductivity relaxation phenomenon, as depicted in Fig. 5.8(j) is what causes the changeover region where frequency-independent conductivity transforms into dispersive conductivity. Based on the jump relaxation model, the frequency-dependent conductivity of the glass system can be analysed further [68], [69]. The extended time interval associated with lower frequencies contributes to dc conductivity, resulting in a plateau region where ions can successfully hop to an unoccupied site nearby.

When an ion makes its "initial hop" to a nearby point, it can either hop back to its original position (correlated forward-backward hopping) or stay in its new position while the ion cloud around it adjusts to the new configuration (cage relaxation). The probability of each of these processes occurring is influenced by the frequency and duration of the applied electric field. At higher frequencies, there is a greater probability of correlated forward-backward hopping occurring, which contributes to the high-frequency dispersion observed in ac conductivity spectra. This is because the ions have less time to relax in their new positions before the electric field changes direction, so there is a higher likelihood that they will hop back to their original positions. On the other hand, at lower frequencies, the cage potential around the ions has more time to relax, which can lead to a decrease in conductivity. This is because the ions are more likely to remain in their new positions as the cage potential adjusts, rather than hopping back to their original positions.

- **Hopping frequency**

Fig. 5.8(a-g) shows that when the temperature rises, the onset frequency of dispersion shifts to the higher frequency side. The frequency at which the relaxation effect begins to dominate and shows the transition from frequency-independent (plateau) conductivity to frequency-dependent conductivity behaviour is known as the hopping frequency. In the case of the NBP glass sample containing 4 $wt.\%\ NaI$ salt, the solid arrow line in Fig. 5.8(j) represents the hopping frequency of mobile cations. According to Jonscher power law, the hopping frequency of ions and the carrier concentration have been estimated from ac conductivity spectra. Almond and West [70]–[72] have developed formalisms based on universal power law [73], using the mathematical expression. Following is the equation of the universal power law representation according to A-W formalism.

$$\sigma'(\omega) \propto \omega \left[\left(\frac{\omega}{\omega_0}\right)^a + \left(\frac{\omega}{\omega_0}\right)^{b-1}\right] \ldots\ldots \quad (5.7)$$

Where, ω_0 is the characteristic frequency, ω_p is hopping frequency and K is a constant, $a = -1$ and $b = n$.

$$\sigma'(\omega) = \mathrm{K}\omega\left[\left(\frac{\omega}{\omega_p}\right)^{-1} + \left(\frac{\omega}{\omega_p}\right)^{n-1}\right] \ldots\ldots \quad (5.8)$$

$$\sigma'(\omega) = \mathrm{K}\omega_p + \mathrm{K}{\omega_p}^{1-n}\omega^n \ldots\ldots \quad (5.9)$$

By comparing power law equation (6) with the above equation (5.9),

$$\sigma'(\omega) = \sigma_{dc} + A\omega^n \ldots\ldots \quad (5.10)$$

$$\therefore \sigma_{dc} = \mathrm{K}\omega_p \ldots\ldots \quad (5.11), \text{ and } A = \mathrm{K}{\omega_p}^{1-n} \ldots\ldots \quad (5.12)$$

From the above Eq. (5.11) and (5.12) $\sigma_{dc} = A{\omega_p}^n$ or $A = \sigma_{dc}/{\omega_p}^n$. Hence, the frequency dependent conductivity can be modified as,

$$\sigma'(\omega) = \sigma_{dc}\left[1 + \left(\frac{\omega}{\omega_p}\right)^n\right] \ldots\ldots \quad (5.13)$$

From the above equation, when frequency which is corresponding to the hopping frequency, $\omega = \omega_p$, the ac conductivity is given as,

$$\sigma'(\omega) = 2\sigma_{dc} \ldots\ldots \quad (5.14)$$

According to the Eq. (5.14), the hopping frequency is the specific frequency at which ac conductivity becomes twice that of the direct current conductivity. Substituting equation (above) into the universal power law yields the hopping frequency as,

$$\omega_p = \left(\frac{\sigma_{dc}}{A}\right)^{\frac{1}{n}} \ldots\ldots \quad (5.15)$$

The hopping frequency (ω_p) against the inverse of temperature $(1000/T)$ for each of the glass composition is shown in Fig. 5.8(k). The rate at which ions attempt to hop from one site to the nearby accessible site increases with an increase in temperature. It confirms the ion migration through the thermally stimulated ion hopping mechanism.

For frequencies above $(\omega > \omega_p)$, ion conduction improves with increasing ω. As depicted in Fig. 5.8(l), the hopping frequency (ω_p) derived from an empirical relationship of the NSPT model and experimentally obtained data is nearly comparable. In addition, the activation energies for ion conduction and hopping are depicted in the inset of Fig. 5.8(l). Across all samples, the activation energy for ion hopping is modest compared to that of the ion conduction process. The inset of Fig. 5.8(l) depicts the glass composition-dependent hopping frequency for ion migration.

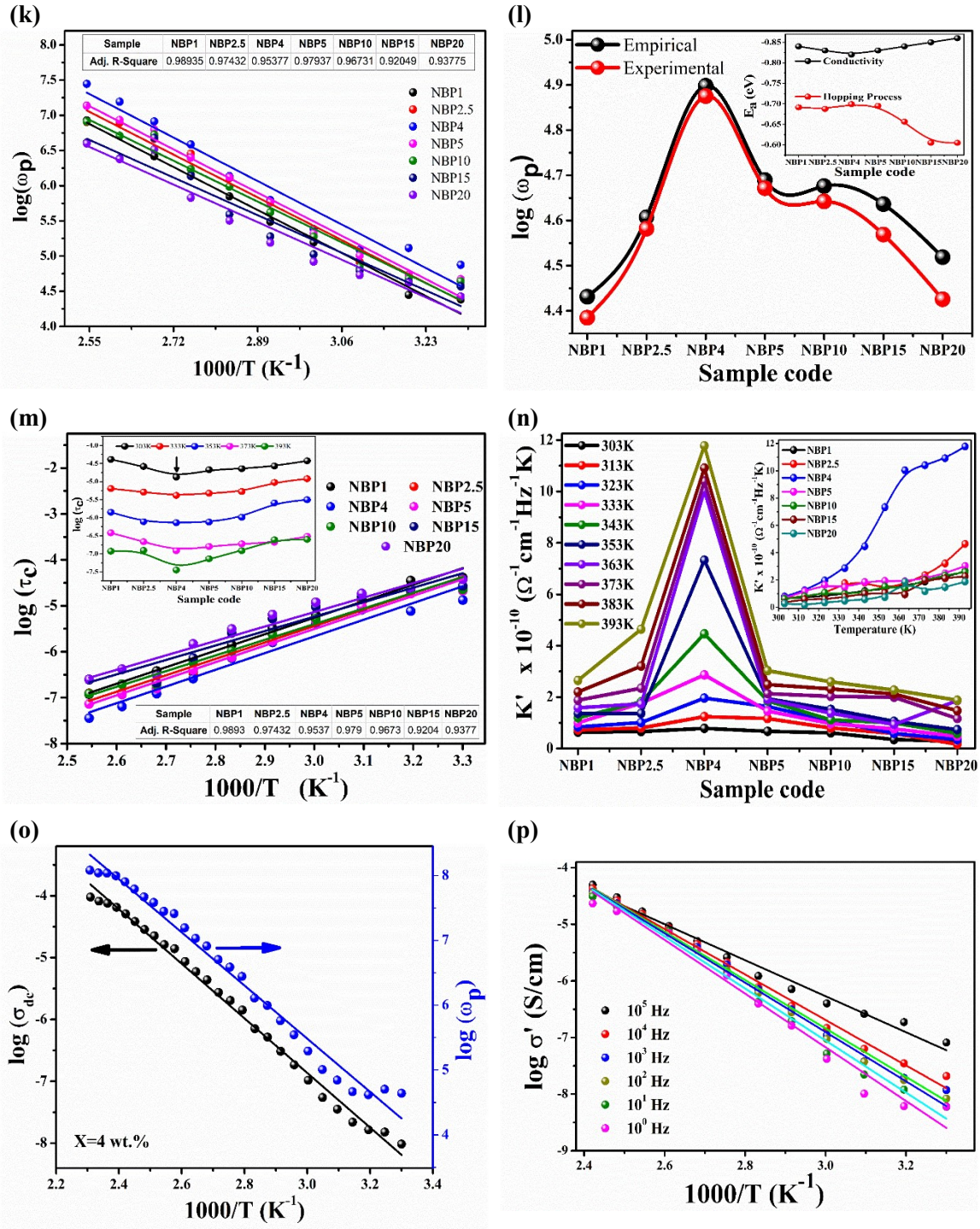

Figure 5.8: *For all the glass compositions of NBP series,(k) The plot of* ω_p *vs* $1000/T$ *exhibits the Arrhenius trend with the activation energy for conduction, (l) Hopping frequency* ω_p *by employing empirical formula of NSPT model and the experimental data. The activation energies for ion conduction and hopping process (inset), (m) Arrhenius behavior of relaxation time when plotted as a function of inverse of temperature and as a function of glass composition the relaxation time is shown in inset, (n) The mobile carrier concentration* K' *at various temperature and as a function of temperature for* $x\ wt.\%\ of\ NaI$ *(inset), (o) Comparative study of dc conductivity and hopping frequency as a function of inverse of temperature for the highly conductive sample of the glass series, and (p) Conductivity variations at various frequencies for the glass compositions containing* $4\ wt.\%\ of\ NaI$.

The hopping frequency is found to be almost reliant on the presence of NaI in the host glass system and follows the compositional variation of bulk conductivity. Fig. 5.8(l) illustrates the fluctuation in activation energies for ion conduction and hopping, and reveals that activation energies for the hopping of ions are lower than those of the conduction process for all samples, suggesting that ions involved in the conduction process probably experience a distinct potential barrier due to the localized electrons of the amorphous matrix. The glass sample with a $4\,wt.\%$ addition of NaI has the lowest activation energy for both conduction and relaxation, obtained using Fig. 5.8(m), suggesting higher conductivity in short time intervals for the relaxation phenomenon.

The mobile ion concentration (K') is one of the determinants of conductivity, calculated from the hopping frequency and the dc conductivity. The relationship between the mobile ion concentration (K') with dc conductivity (σ_{dc}), temperature (T) and hopping rate $\left(\tau_c = 1/\omega_p\right)$, as given by Almond et al; [74], is as follows (Eq. 5.16).

$$K' = \frac{\sigma_{dc}\,T}{\omega_p} \ldots\ldots (5.16)$$

As shown in Fig. 5.8(n), the plots of K' versus NaI content and as a function of temperature, inset of Fig. 5.8(n), respectively, demonstrate that mobile carrier density increases with NaI concentration and also exhibits temperature-dependent behaviour.

The increase in mobile ion concentration K' is attributed to the increase in conductivity that occurs with the addition of dopant salt. The carrier concentration rate significantly increased for the composition with $4\,wt.\%$ NaI added, but the fluctuation of the mobile carrier concentration K' with temperature is insignificant for the other compositions, except for NBP4 which is thermally activated. However, the temperature-dependent hopping rate of mobile ions may still cause some variation in conductivity for all compositions. As the hopping rate increases with temperature as shown in Fig. 5.8(o), the conductivity of the present glass system increases as expected. It is intriguing to note from Fig. 5.8(p) that, at various frequencies, the conductivity of the NaI-doped NBP glass system follows Arrhenius behaviour.

The activation energy determined from the frequency-dependent Arrhenius plots agrees well with the conductivity plot calculated during impedance analysis. This characteristic is consistent with the Jonscher power law analysis of ac conduction conductivity.

Conductivity scaling

The scaling of conductivity parameters is a useful tool for understanding the ion conduction mechanism in glass systems. The conductivity of a material is typically affected by its composition and temperature. By scaling the conductivity spectra, researchers can more easily compare the behavior of different glass systems and gain insight into the underlying physical mechanisms responsible for their conductive properties [75]–[81]. Summerfield [79] was the first to attempt scaling of the sigma spectra for semiconducting materials. Since then, many researchers have developed distinct scaling formulas for the ac conductivity spectra of various ion-conducting glass systems. One of the most widely used scaling approaches was developed by Roling et al. [80], [82], and modified by other researchers [82]–[84]. This method involves scaling the frequency and magnitude of the conductivity spectra using a characteristic frequency and a characteristic conductivity value. Following Eq. (5.17) is an explanation of the Summerfield scaling in its most elementary version.

$$\frac{\sigma'}{\sigma_0} = F\left(\frac{f}{\sigma_0 T}\, x\right) \ldots\ldots \quad (5.17)$$

Where, f is the frequency, σ_0 is the conductivity at a given temperature, T is the absolute temperature, x is concentration (of dopant) factor. At $\omega = \omega_p$, the ac conductivity can be equated with dc conductivity as given in Eq. (5.14). The scaling formalism, Eq. (5.18), given by Roling in which the consideration of the simplest case where charge carriers remain constant with temperature and hence from Eq. (5.16), one can write it as ω_p is thermally activated factor with the same quanta of energy as $\sigma_{dc}T$.

$$\frac{\sigma'}{\sigma_0} = F\left(\frac{f}{\sigma_{dc}T}\right) \ldots\ldots \quad (5.18)$$

The universal function F, which is indifferent to changes in temperature and chemical composition, describes the ion dynamics in this equation. The most significant benefit of such scaling law is that it uses the quantities that are already available as scaling parameters.

As illustrated in Fig. 5.9(a-f) and (g-l), the ac conductivity (σ') data is scaled by dc conductivity (σ_{dc}), while the parameters $\sigma_{dc}T$ or say ω_p (Eq. 5.17), and $\sigma_{dc}T_x$ (Eq. 5.18), are respectively utilised to normalise the frequency axis. The ac conductivity spectra, as shown in Fig. 5.9(a-l), for different temperatures, are almost perfectly merged into a single master curve, indicating the presence of a Time-Temperature Superposition (TTS) and a temperature-independent conduction mechanism, also known as canonical scaling by Sidebottom [84].

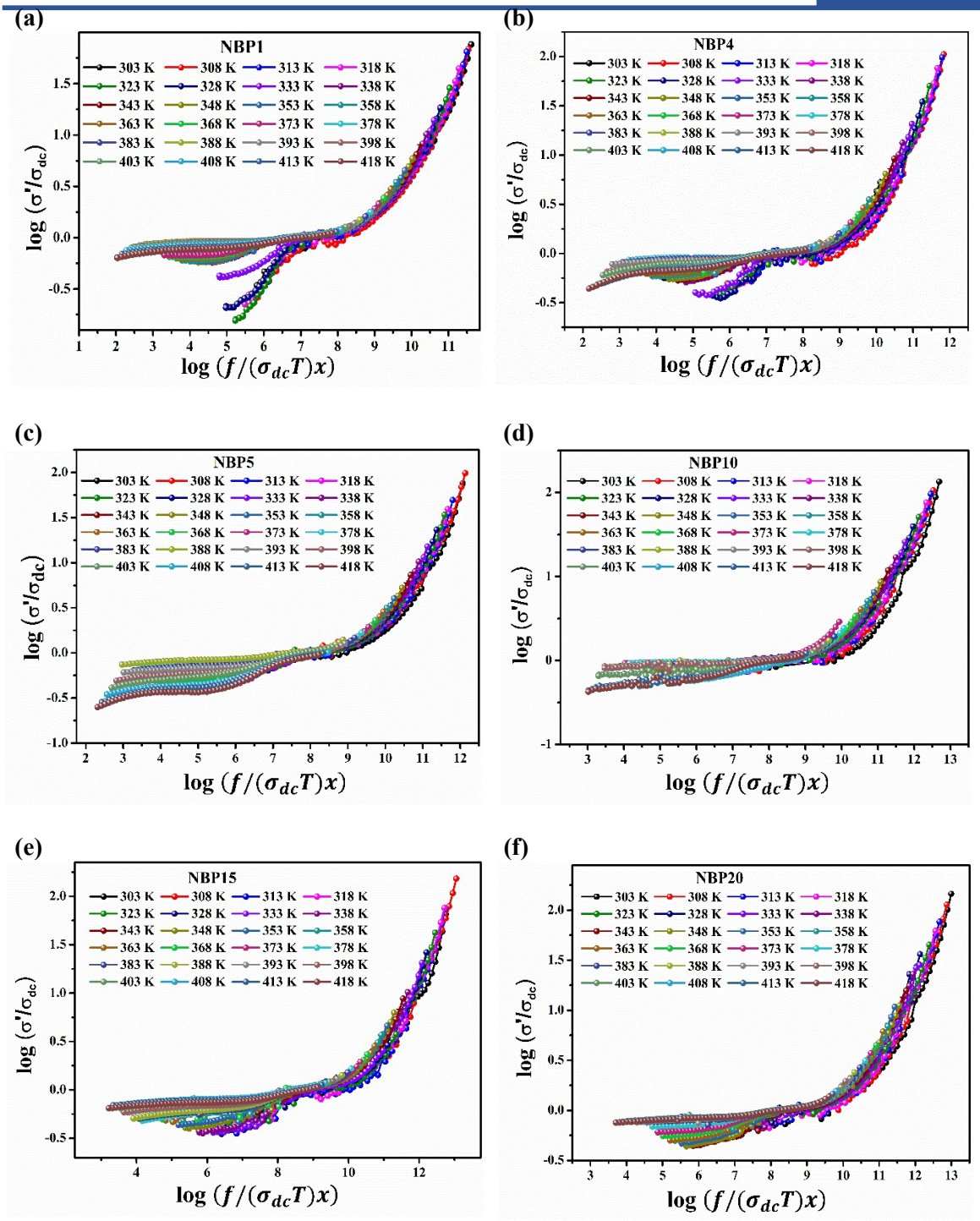

***Figure 5.9**:(a-f) Plots of normalized conductivity spectra with frequency using Summerfield formulation at different temperatures for various glass compositions.*

However, the spectra do not merge and fall into a master curve at very low frequencies near the polarization region, as shown in Fig. 5.9(a-l), due to a change in the Na^+ ion concentration and slightly varied ion transport behaviour in the glass at a specific temperature.

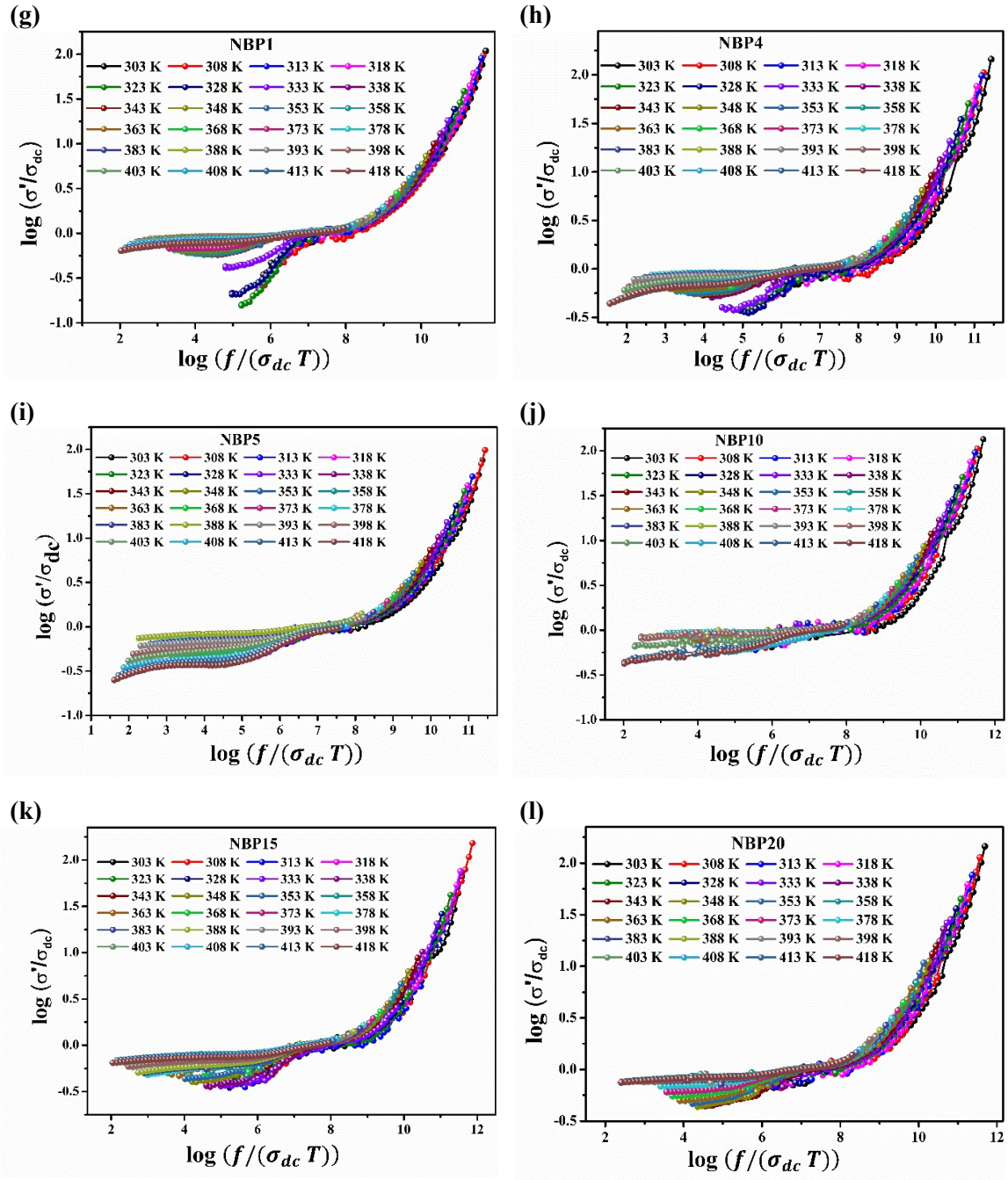

***Figure 5.9**:(g-l) Plots of normalized conductivity spectra with frequency using Roling formulation at different temperature for various glass compositions.*

Canonical scaling is a principle that predicts the behavior of the frequency-dependent electrical conductivity of a material as a function of temperature, frequency, and ion concentration. According to this principle, when the temperature is changed, but the ion concentration and material structure remain constant, the shape of the ac conductivity spectrum is preserved. This means that the conductivity spectrum can be scaled by a characteristic frequency and temperature, and the behavior of the spectrum can be predicted by studying its behavior at a single frequency and temperature [82], [85]–[87].

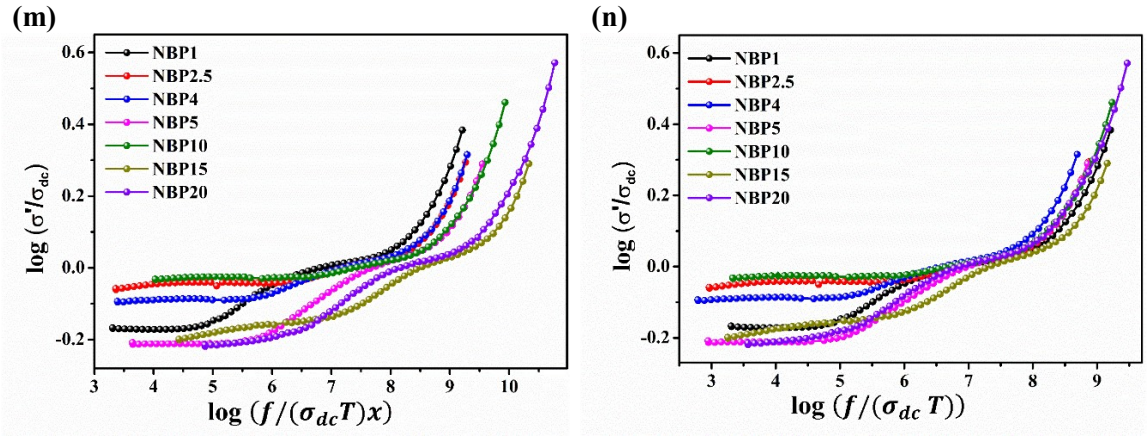

***Figure 5.9**: (m-n) Plots of normalized conductivity spectra with frequency using Summerfield and Roling formulation at 373K for various glass compositions.*

However, in some materials such as disordered glasses and crystals that conduct electricity through single ions, the temperature-dependent conductivity spectrum does not follow canonical scaling. Instead, these materials exhibit a phenomenon known as temperature-time superposition (TTS). TTS means that the conductivity spectra measured at different temperatures can be shifted and scaled to coincide at high frequencies, indicating that the material's relaxation dynamics are temperature-independent at high frequencies. The TTS behavior in disordered glasses is attributed to the large distribution of energies associated with the ion sites and barrier heights, which causes a broad distribution of jump rates of the ions. These jumps are governed by Coulombic interactions between the ions, which are affected by the potential energy landscape of the material.[88], [89].

Fig. 5.9(m-n) depict the scaling of ac spectra as a function of frequency scaling using the Summerfield and Roling formulations, respectively, for various NaI concentrations at a temperature 373 K to demonstrate the effect of the mobile ion concentration (Na^+) and modification in the glass structure.The sigma spectra for various compositions do not superimpose on a single master curve. However, the scaling formulation suggested by Roling nearly agrees with the data of the investigated system as compared to the Summerfield formalism. As demonstrated in Fig.5.8(n), the concentration of mobile ions, denoted by K', increases with the NaI amount, eventually reaching its highest value in the NBP4 sample. According to Roling [80], ion concentration variation substantially affects the ion relaxation phenomenon. As a result, scaling as a function of composition is typically observed in glasses with significant variations in mobile ion concentration that change with glass composition, suggesting that the compositional range under study may not have probably homogenous Na^+ ion conduction.

c) Dielectric Study

Dielectric analysis is a useful technique for investigating the properties of materials that conduct electricity, particularly ion-conducting materials. In these materials, the polarization process (which arises from the reorientation of local ions) and the conduction process (which involves the movement of ions) are intimately linked, making it difficult to distinguish between them [90]. Dielectric formalisms of impedance spectroscopy can be used to study the dipolar relaxation in both solids and liquids. In this process, the reorientation of permanent dipoles produces frequency-dependent dielectric permittivity characteristics. By analyzing these characteristics, researchers can gain insight into the underlying mechanisms of ion transport in ion-conducting materials [83].

The following is the Eq. (5.19-5.21) for the complex dielectric formalism ε^*, which is related to complex impedance and complex conductivity functions and is given in detail in Chapter 3.

$$\varepsilon^*(\omega) = \frac{1}{i\omega C_0}\left(\frac{1}{Z^*}\right) \ldots\ldots \quad (5.19)$$

$$\varepsilon^*(\omega) = \frac{\sigma^*(\omega)}{i\omega\varepsilon_0} \ldots\ldots \quad (5.20)$$

$$\varepsilon^*(\omega) = \varepsilon'(\omega) - i\varepsilon''(\omega) \ldots\ldots \quad (5.21)$$

Where, $\omega = 2\pi f$ is the radial frequency, ε_0 is the permittivity of free space, and the parameter $C_0 = \varepsilon_0(a/t)$ that depends on cross section (a) are and the thickness (t) of the specimen.

It is a common fact that many liquids and solids have strong frequency dependence on their dielectric constants. ε_0, a static value at low frequencies, is generally found to be the dependence, which decreases to ε_∞, a smaller limiting value, at higher frequencies. Two characteristic phenomena, dispersion and absorption, occur in an inhomogeneous dielectric medium. The complex dielectric constant explains why there is an "absorption conductivity" in the transition area of anomalous dispersion (Eq. 5.21) [90].

Debye's theory explains that the dipole polarization of the molecules is responsible for the difference between ε' and ε". In an alternating current field, the dipole polarization of the molecules is opposed by thermal motion and other factors such as chemical interactions. This results in viscous damping, which is the dissipation of energy due to the frictional forces between the molecules. Debye treated the molecules as spheres in a continuous liquid with macroscopic viscosity, which lead to derive a mathematical model for the dielectric.

The real and imaginary parts of the Complex dielectric function (ε^*) are given as follows.

$$\varepsilon' = \frac{-1}{\omega C_0}\left(\frac{Z''}{Z'^2 + Z''^2}\right) \ldots \quad (5.22), and \quad \varepsilon'' = \frac{-1}{\omega C_0}\left(\frac{Z'}{Z'^2 + Z''^2}\right) \ldots \quad (5.23)$$

For an ideal Debye system, the real part, ε', corresponds to the dielectric constant, and it changes in steps from a lower to a higher frequency, with two plateau regions. The lower frequency plateau region is called ε_s, and the higher frequency plateau region is called ε_∞. At a low-frequency regime, the $\varepsilon'(\omega)$ plot enables the determination of the static dielectric constant, also known as the low-frequency permittivity value (ε_s). At higher frequencies, the periodic reversal of the applied electric field happens quickly, and therefore no extra ionic jump in the field direction occurs. In the meantime, the polarization due to the accumulated concentration of mobile ions at high energy barrier sites disappears, and the measured value of ε' saturates at ε_∞. Furthermore, $\Delta\varepsilon = \varepsilon_s + \varepsilon_\infty$ represents the change in dielectric permittivity, indicating dielectric strength, and is the result of all relaxation processes [91].

The manifestation of the movement of mobile ions due to the application of an electric field across a material corresponds to dielectric loss, $\varepsilon^{"}$, which is an imaginary part of dielectric formalism. Due to their significant inertia, the mobile ions are incapable of responding to the abrupt reversal of the applied electric field. And they lag in responding to the applied electric field, which causes a loss peak on the high-frequency side.

The resulting ε' spectra, shown in the Fig. 5.10(a-f), have three distinctive regions: a low-frequency plateau (ε_s), a mid-frequency dispersion, and a high-frequency saturation plateau (ε_∞). For all the glass compositions, the mid-frequency dispersion and high-frequency saturation are clear, while the low-frequency plateau is evident for NaI concentration $x = 1$ to $5\ wt.\%$ from $303\ K$ to $373\ K$. At higher temperatures, polarization caused the low-frequency plateau to merge with the dispersive region in all compositions of glass, making it difficult to distinguish them in all samples. From Fig. 5.10(a-f), it is seen that the dielectric constant (ε'), particularly at low frequencies ($50\ Hz - 1\ kHz$), increases with temperature in all glass compositions. As the temperature rises, a similar change accompanied by an increase in the ε' value is observed. These results are consistent with what earlier researchers observed [59], [92]–[94]. All of these systems are observed to have rather high ε' values. Such high values are a result of the high ionic conductivity of the material. It has been noted that most solid electrolytes have a high dielectric constant [95]–[97].

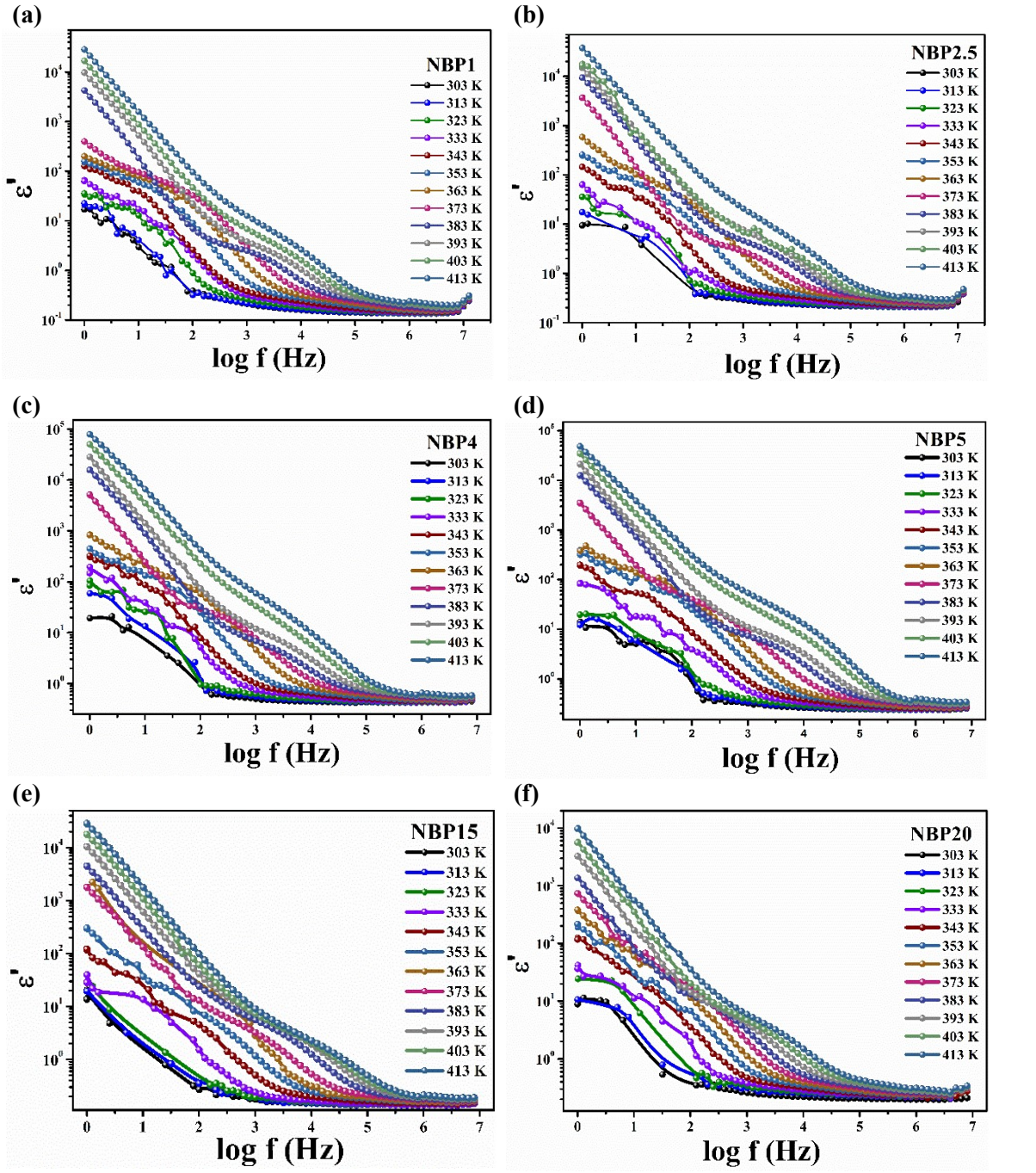

***Figure 5.10**:(a-f) Plots of dielectric constant (ε′) spectra with frequency at different temperature for various glass compositions.*

The phenomenon of electrode polarization can occur when an electrical potential is applied across an electrode-electrolyte interface [98]. In this case, the mobile ions in the electrolyte are blocked by the electrode and accumulate at the interface, resulting in a charge separation and an electric field. This can affect the behavior of the ions and the overall performance of the system.

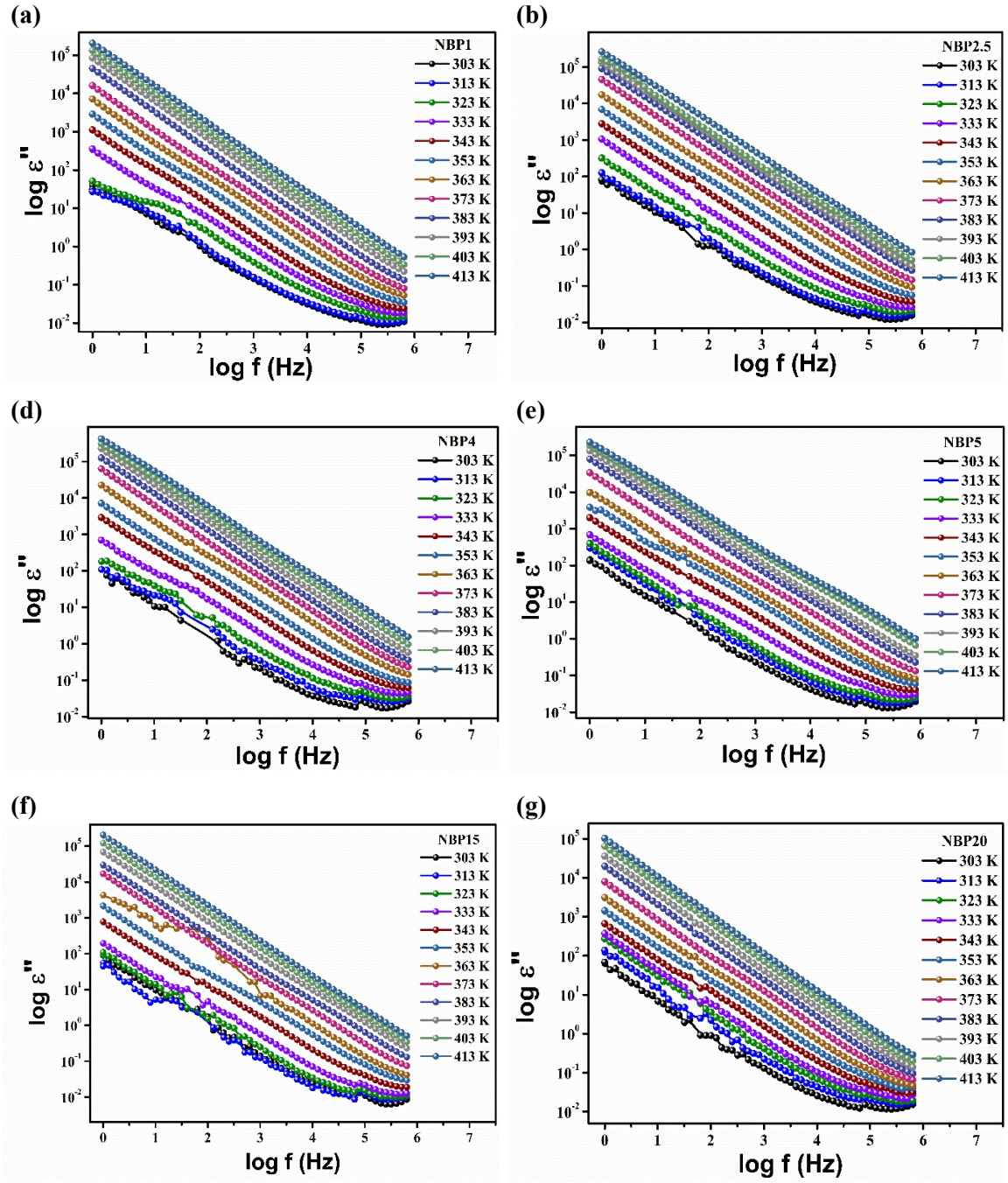

***Figure 5.11**:(a-f) Plots of dielectric loss (ε") spectra with frequency at different temperature for various glass compositions.*

The accumulation of mobile cations at the interface can be related to the free energy barriers that prevent ion motion in the glassy sub-lattice. These barriers can vary in size and shape, resulting in a distribution of relaxation times, which is characteristic of the Stevels model of dielectric relaxation in glasses [60]. Thus, the change in ε' at lower frequencies is caused by the long-distance diffusion of Na^{+} ions, which involves a series of jumps over barriers of variable heights. The periodic reversal of the field occurs so quickly at higher frequencies that there are no extra ionic jumps in the field direction.

As observed in the current system, the polarization caused by charge accumulation at high-frequency barrier sites disappears, the contribution of mobile ions to dielectric ε'decreases to ε_∞, and an increase in conductivity is anticipated. Fig. 5.11(a-f) depicts the imaginary component of permittivity ε''as a function of frequency at various temperatures for the NBP glass system to analyze the influence of sodium iodide dopant salt on the dielectric loss spectrum (ε'').

ε'', or dielectric losses, have no peak unless the dc conductance is eliminated, which is only conceivable for low-conducting materials. It suggests that the behavior of dielectric losses with respect to temperature is not the only factor affecting their behavior. The presence of dc conductance can also impact the behavior of dielectric losses. The elimination of dc conductance is not always possible, especially in materials that are highly conductive. Similar properties have been observed in other glasses that conduct Ag^+ ions, suggests that the behavior of dielectric losses is not limited to a particular type of material. Other glasses that conduct ions have also exhibited similar behavior in terms of variations in ε' and ε''. These variations suggest a Non-Debye trend, which is characterized by the presence of space charge regions and their behavior with respect to frequency [99], [100].

As previously stated, conductivity is thermally stimulated and rises with increasing temperature. No loss peak is observed for any of the glass samples in the examined frequency range. The high dielectric loss in materials confirms to the characteristics of all high ionic conducting materials. The high value of the dielectric constant is attributed primarily to the high ionic conductivity and significantly less to the electronic conductivity [97]. In such materials, the dielectric loss is roughly two orders of magnitude more than the dielectric constant. Fig. 5.12(a-b) show the temperature dependence of the real and imaginary part of permittivity for various frequencies within the interval of 10 Hz to 1 MHz for 1 $wt.\%$ of NaI in the NBP glass system. At lower frequencies, between 10 Hz and 10 KHz, both ε' and ε''increase as the temperature rises. Increases in ε' and $\varepsilon''$are much less pronounced at frequencies above 10 KHz compared to lower frequencies. At low frequencies, as the temperature rises, the mobile ions are free to hop parallel to the applied field, resulting in an increase in permittivity components. For higher frequencies in the given temperature range, the charge carriers are insufficiently free to follow the changing electric field; therefore, the real and imaginary components ($\varepsilon'$and ε'') of permittivity are almost constant. The similar trends of ε' and ε'' also can be observed for 1 MHz frequency plots for the glass sample, as shown in Fig. 5.12(c-d).

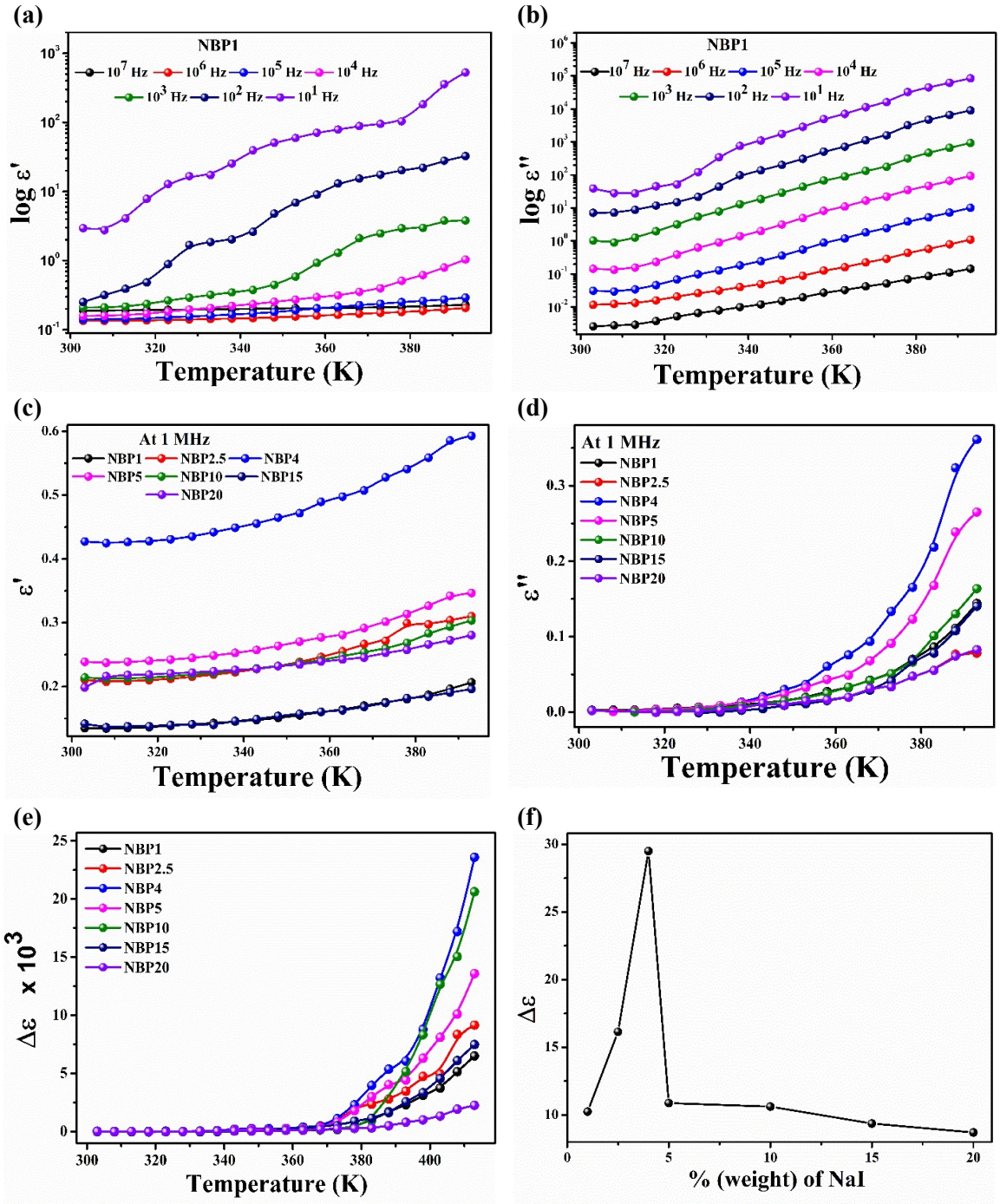

***Figure 5.12**: Plots of temperature dependence of the dielectric constant (ε') and the dielectric loss (ε''), (a-b) for several values of frequencies, (c-d) At $1MHz$ frequency for all the samples. The dielectric strength ($\Delta\varepsilon$), (e) as a function of temperature for all compositions of glass series, and (f) as a function of x $wt.\%$ of NaI at 303 K temperature.*

At lower frequencies, the polarization of an ionic medium is mainly determined by the movement of mobile ions in the direction of the applied electric field. When the frequency of the applied electric field is low enough, mobile ions such as sodium ions (Na^+) can easily escape from sites with low energy barriers in the direction of the electric field, leading to a relatively high polarization magnitude or dielectric relaxation strength ($\Delta\varepsilon$) of the

medium. However, at high frequencies, the motion of the mobile ions is impeded by the high energy barriers encountered at certain sites in the medium, causing them to accumulate at those sites. This results in a lower polarization magnitude or dielectric relaxation strength ($\Delta\varepsilon$) of the medium. The dielectric relaxation strength as a function of glass composition and temperature are shown in Fig. 5.12(e-f) respectively. The dielectric relaxation strength ($\Delta\varepsilon$) is thermally caused and exhibits a progressive increment with temperature, as seen in the figures. The resulting polarization is caused by microscopic events and is influenced by the concentration of mobile ions as well as the hopping distance.

Typically, the so-called loss tangent ($\tan\delta$) or dielectric loss angle of a system defines the ratio of the energy dissipated per radian in the material to the stored energy at the point of polarization peak, given by Eq. 5.24.

$$\tan\delta = \frac{\varepsilon''_{(\omega)}}{\varepsilon'_{(\omega)}} \quad \ldots\ldots\ldots\ldots (5.24)$$

From the plot of $tan\,\delta$ versus $log\,f$ is shown in Fig. 5.13(a-f) for all NBP glass compositions at various temperatures, it can be observed that the value of $\tan\delta$ is nearly constant or temperature independent at lower frequencies and rapidly decreases at higher frequencies until it appears to flatten at ~ $10^7\ Hz$ and above. When the temperature rises, the $\tan\delta$ plot shows that the frequency disperses toward higher frequencies.

Furthermore, it seems that as the temperature increases, the $\tan\delta$ plot shifts towards higher frequencies, which is known as frequency dispersion. This behavior is often observed in materials with a relaxation process, where the relaxation time decreases as the temperature increases, leading to a shift in the frequency of the maximum loss (or peak) towards higher frequencies. The inset of Fig. 5.13(f) illustrates the relationship between $\tan\delta$ and $\log f$ for various dopant concentrations at ambient temperature.

When the dopant concentration increases, the dispersion region shifts to higher frequencies, as shown in the graph. Additionally, the rapid drops in $\tan\delta$, followed by a constant value at higher frequencies, demonstrate that $\tan\delta$ is inversely proportional to some frequency power. Fig. 5.13(g) shows the plot of dielectric relaxation time and conductivity relaxation time versus inverse of temperature for 4 $wt.\%$ of NaI in the sodium oxide borophosphate glass structure.

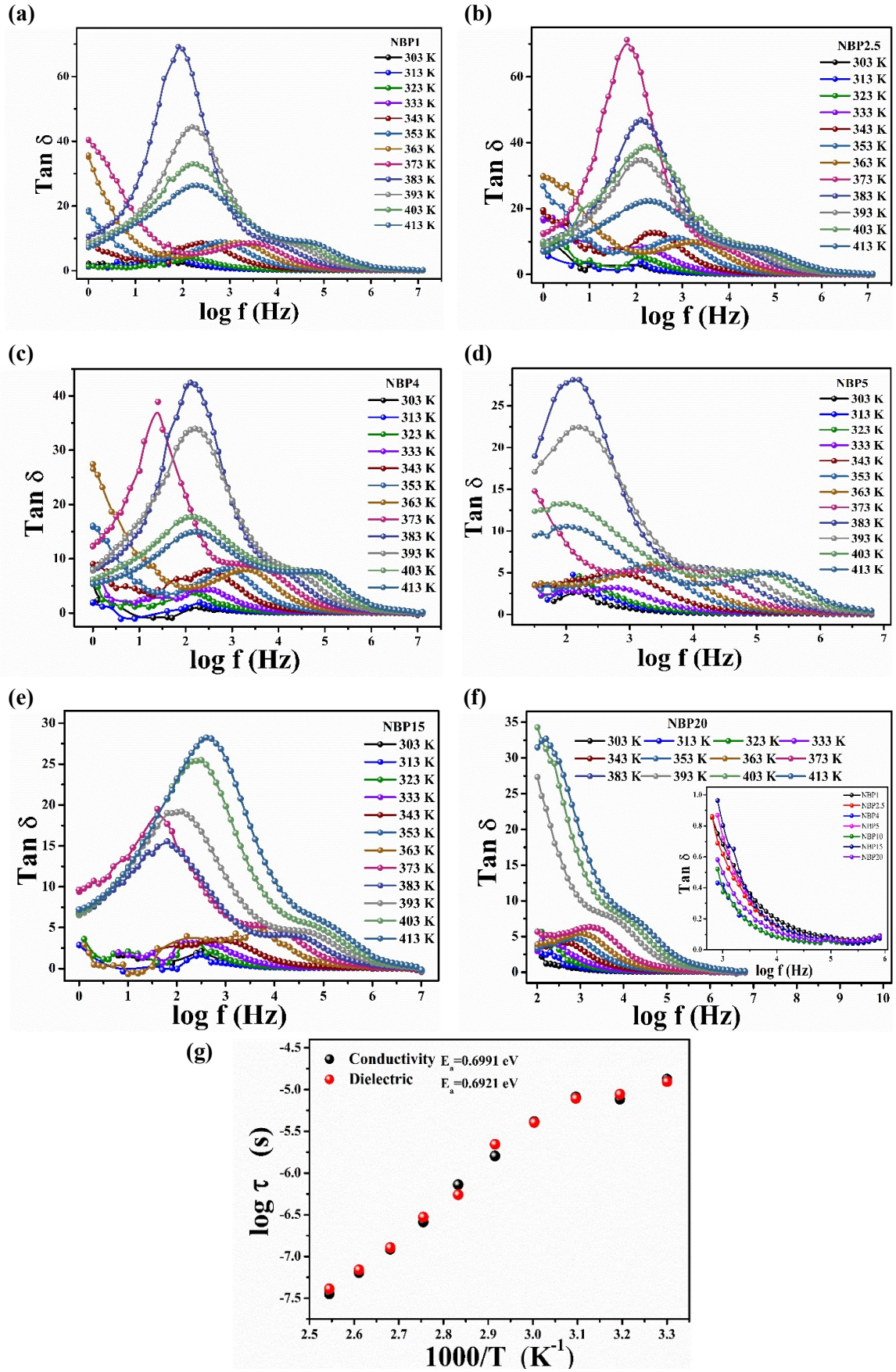

***Figure 5.13**:(a-f) Plots of $\tan\delta$ spectra with frequency at different temperature for various glass compositions (Inset of Fig. f: $\tan\delta$ spectra vs log f for NBP series samples), (g) Conductivity and Dielectric Relaxation time (τ) versus $1000/T$ plot for the NBP4 glass system.*

The activation energy (E_a) obtained from the relaxation plot (τ) is nearly the same as that obtained from the corresponding conductivity plots, which suggest that the relaxation time is determined by the flow of charge carriers. Thus, it is possible to say that the motion of mobile charge carriers, Na^+ ions in the present case are possible for both conductivity and relaxation effect.

d) Electric Modulus Study

The modulus is termed as complex electrical modulus, M^* which is related to complex dielectric constant ε^* and complex impedance by the given Eq. 5.25.

$$M^* = \frac{1}{\varepsilon^*} = j\omega C_0 Z^*$$

$$M^* = M' + iM''$$

$$= \left(\frac{\varepsilon'}{\varepsilon'^2 + \varepsilon''^2}\right) + i\left(\frac{\varepsilon''}{\varepsilon'^2 + \varepsilon''^2}\right) \ldots\ldots \quad (5.25)$$

The advantage of using the modulus formalism is that it eliminates such frequency-dependent dielectric conductivity data that arises due to inevitable electrode polarization (contact or interfaces), Maxwell-Wagner effects, or a high dielectric constant.

The Modulus Formalism is a mathematical technique used to analyze relaxation spectra [101] in order to better understand the behavior of materials under varying conditions. It was first introduced by Macedo et al. [60] as a way to distinguish between relaxation and polarization effects in the context of conductivity measurements. The technique involves transforming the frequency-dependent conductivity, $\sigma'_{(\omega)}$, into a representation that exhibits a peak in the modulus of the complex conductivity $M'_{(\omega)}$ by taking the absolute value of the complex conductivity and differentiating it with respect to frequency. This transformation allows for a clearer separation of relaxation behavior from polarization effects, which can be difficult to distinguish using traditional conductivity measurements. The scaling behavior of the data is more evident in the modulus representation. When the concentration of dopant salt NaI is varied against the host glass former, the frequency-dependent actual component of the modulus, $M'_{(\omega)}$, for all compositions of the NBP glass series are in Fig. 5.14(a-f) at different temperatures. The figures display that the $M'_{(\omega)}$ spectra disperse up to 2 MHz. While the real part of modulus spectra tends to saturate to zero at lower frequencies, showing that the electrode polarization contributes negligibly to M^* and that the dispersion is primarily due to conductivity relaxation.

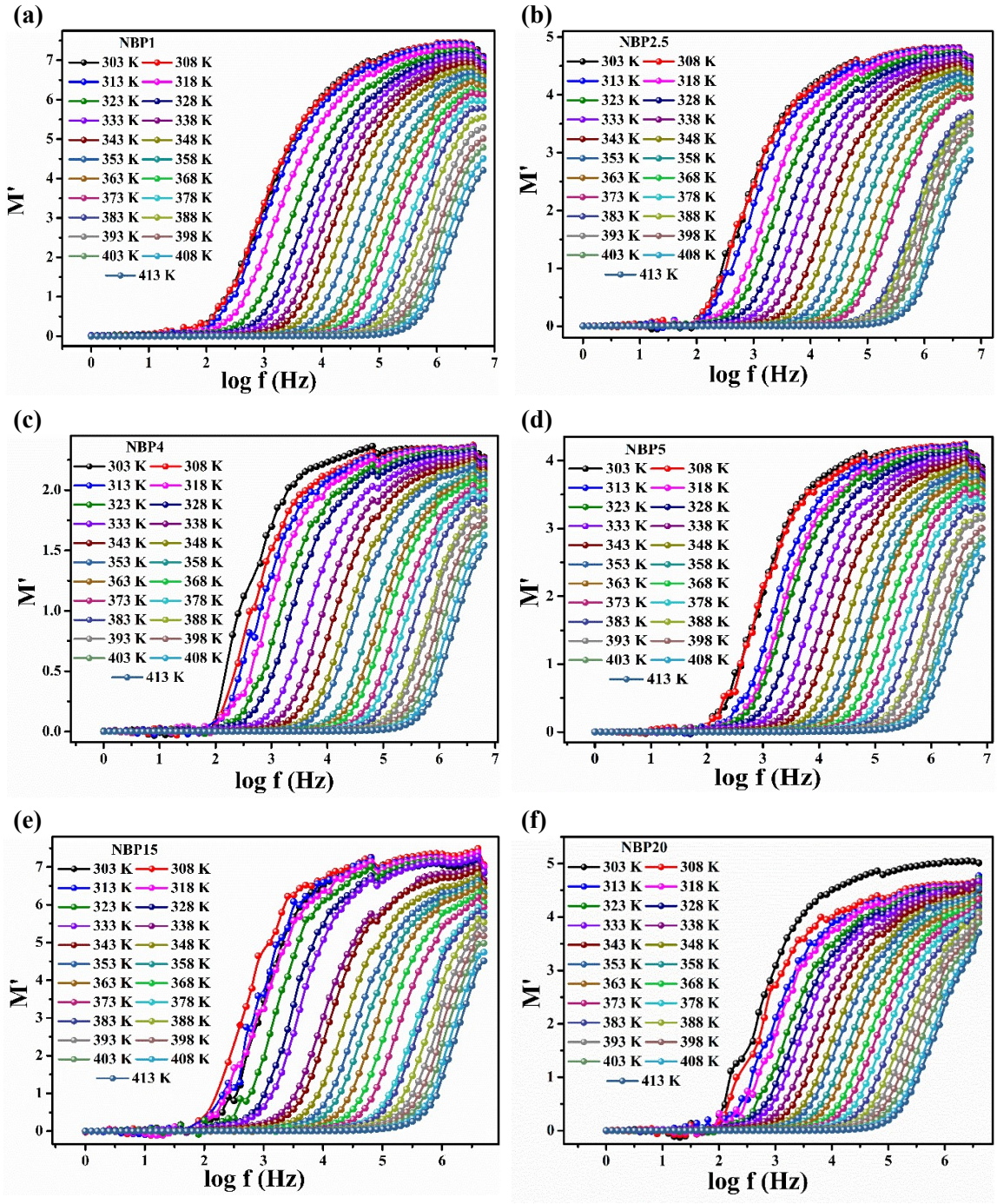

***Figure 5.14**:(a-f) Real part of modulus spectra vs $\log f$ for NBP series samples at various temperatures.*

At higher frequencies, $M'_{(\omega)}$ achieves a stable maximum value. $M'_{(\omega)}$ levels out at higher frequencies at higher temperatures because the relaxation process spreads over a range of frequencies. High-frequency saturation is observed in all the glass compositions. A low-frequency plateau is indicative of suppression of polarization effects. It is also apparent that the beginning frequency of dispersion shifts towards higher frequencies as the NaI

concentration increases up to $x = 4\ wt.\%$. It indicates that as the concentration of mobile ions increases, the mobile Na^+ ion may spend the least time at its relaxing sites.

The absence of high-frequency saturation in these compositions suggests that it may occur beyond the upper frequency limit of the measured range. As the temperature rises, the onset frequency of dispersion moves towards higher frequencies, indicating that thermal activation is involved in this event, and the same effect is observed across all glass compositions. Sample NBP4 shows the plateau and saturation effects of both the lower and the higher frequency regimes, respectively.

Fig. 5.15(a-f) depicts the variation of the imaginary component of modulus $M^{"}$against frequency (often referred to as the modulus spectrum) for all series samples at various temperatures. In contrast to the M' curve, the $M^{"}$ shape typically has an asymmetric peak. Due to the enormous capacitance associated with the electrodes, the spectra have an extended tail at low frequencies. With an increase in temperature, the shape of the curve remains unchanged, but the peak frequency of the modulus $M^{"}_{max}$ shifts to the higher frequency side.

In addition, neither the peak shape nor the peak height i.e. $M^{"}_{max}$ appear to change with temperature variations. The frequency at which the maximum in $M^{"}$ occurs, f_{max} or ω_c, indicates the shift from short-range to long-range mobility at decreasing frequency. The f_{max} notably shifts towards higher frequency with increasing temperature, indicating thermally induced relaxation of mobile sodium ions. In the frequency regime below $M^{"}_{max}$, the charge carriers are mobile over long distances and contribute to dc conductivity. However, on the higher side of f_{max}, mobile charge carriers are constrained by their potential wells and can only make short distance hops. The conductivity relaxation time is related to the peak frequency of relaxation, f_{max}, using the following equation [59], [102], [103].

$$\omega\tau = 1 \quad \ldots (5.26)$$

Where, ω is the peak frequency of $M^{"}$ spectra also known as $M^{"}_{max}$, or f_{max} and relaxation time is given as τ (τ_c occurs at peak frequency). Fig. 5.16(a) depicts the frequency corresponding to $M^{"}_{max}$, $\log f_{max}$or $\log \tau_c$versus reciprocal temperature plot for all the glass samples, which follows the Arrhenius law.

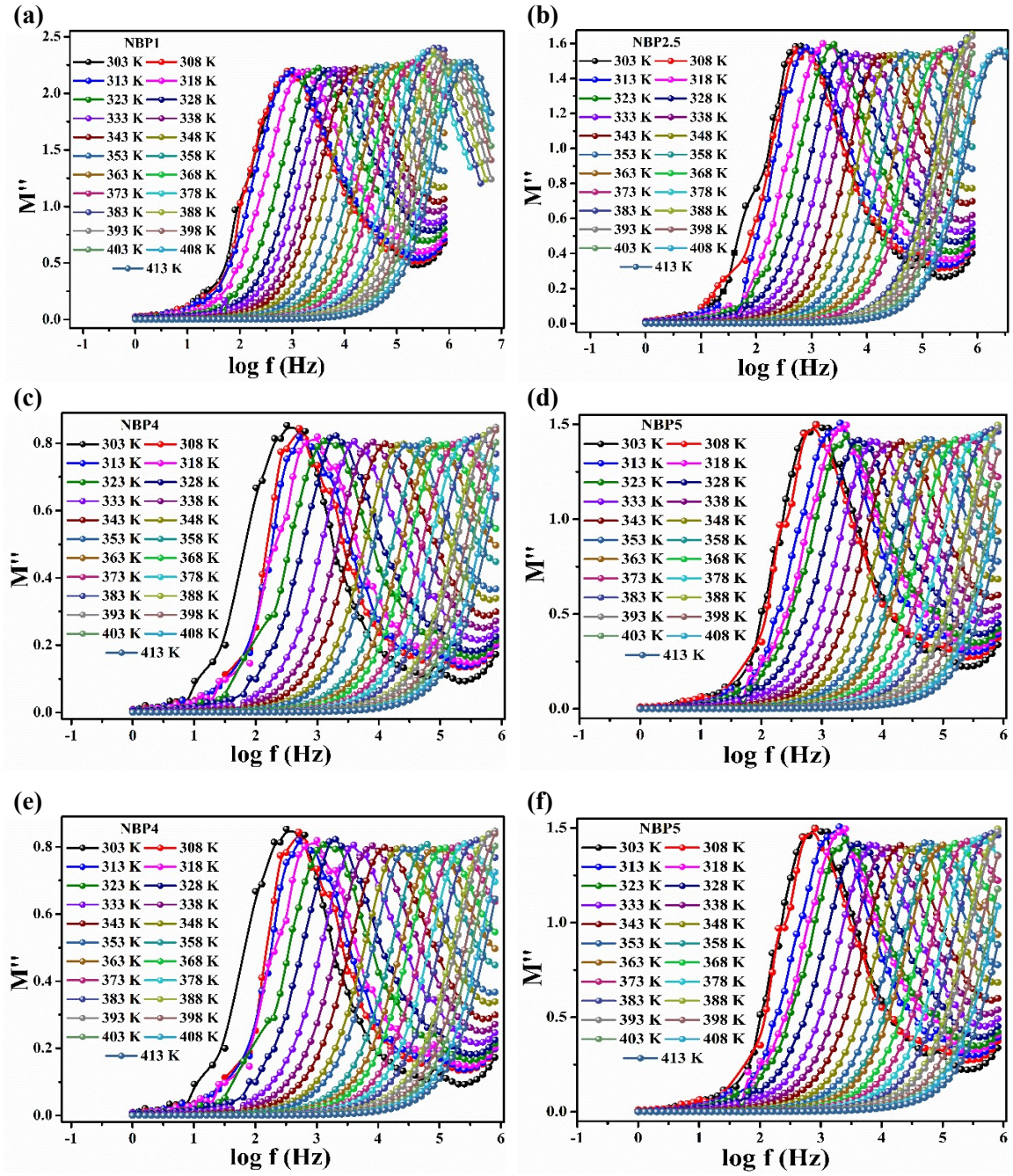

***Figure 5.15**: (a-f) Imaginary part of modulus spectra vs $\log f$ for NBP series samples at various temperatures.*

The value obtained from the impedance spectrum (E_σ) for long-range charge transport and the activation energy derived from the modulus spectrum (E_τ) for short-range migration are comparable and found to be almost the same in magnitude. Since the values of E_τ and E_σ are the same, this implies that the sodium ion transport in the current system, as shown in Fig. 5.16(b), is through hopping mechanisms, regardless of whether the carriers are migrating for long- or short-range.

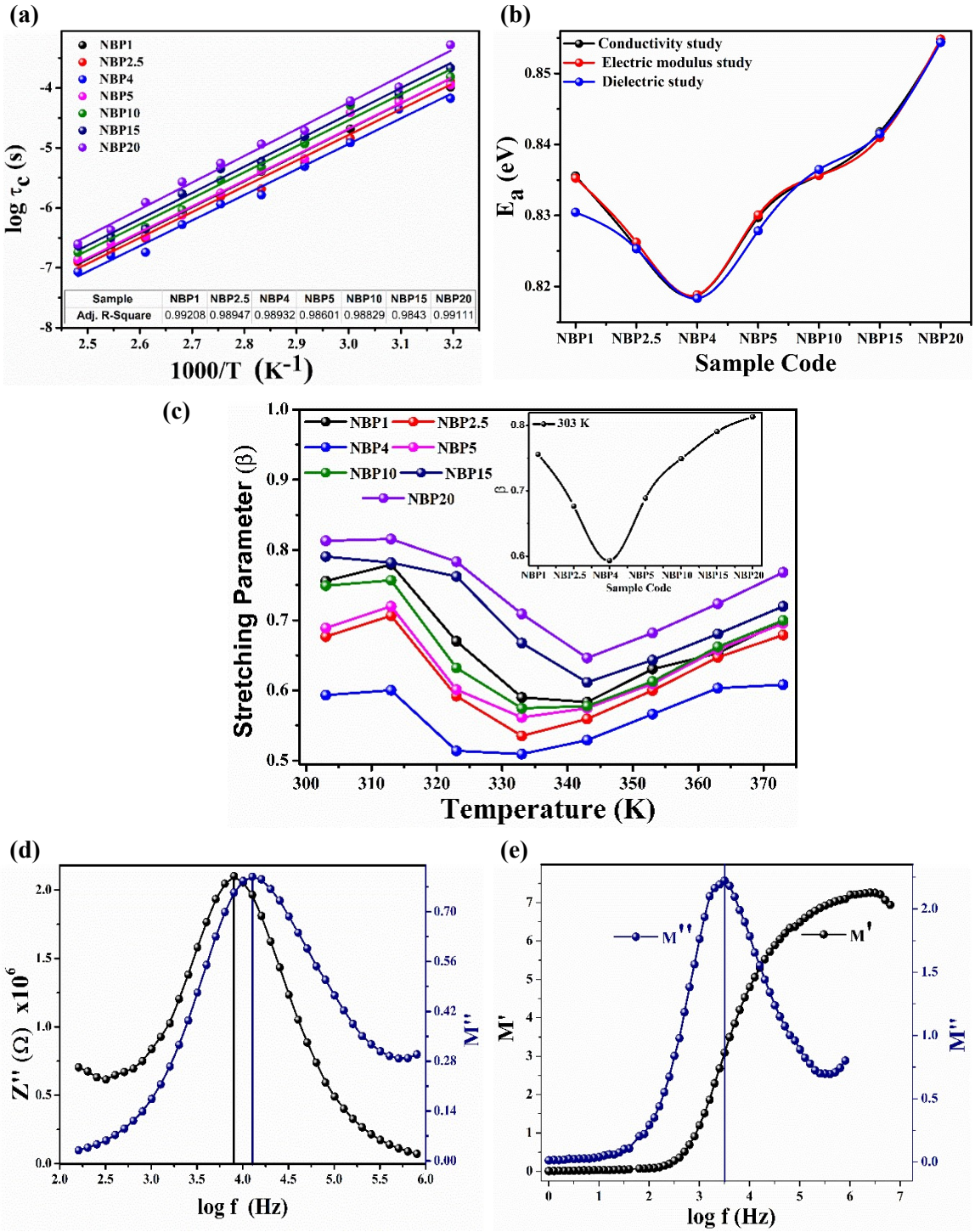

Figure 5.16*:(a) Arrhenius behavior of electric modulus relaxation time, (b) Comparison of activation energy obtained from conductivity, dielectric and electric modulus study, (c) Stretching parameter as a function of temperature (inset: Room temperature trend of β for all glass samples),(d) Imaginary part of impedance and modulus as a function of frequency at 343 K for NBP4 sample, (e) Real and imaginary part of modulus at 323 K for NBP1 sample.*

The full width at half maxima (FWHM) increases with the dopant amount ranging from $x = 1\ to\ 4\ wt.\%$ is quite visible in the Fig. 5.15(a-f). According to the ideal Debye function, the full width at half maximum (FWHM) demonstrates 1.14 decades of

magnitude. In the current system, the FWHM value is greater than 1.14 decades, indicating a distribution of conduction process relaxation time [102]. According to Hasz [104], the distribution of relaxation time is caused by the distribution of free energy barriers for ionic jumps, in which the distribution increases with increasing disorder. However, Grant proposed that the distribution of relaxation times is not a result of the disordered structure of glasses but rather of the cooperative nature of the conduction process [105]. The plot of the normalized modulus is asymmetric, which is consistent with the non-exponential behavior of the electrical function. Moynihan describes the modulus function using the KWW exponential function [106]–[108]. β is a parameter that is derived from fitting the $M^{''}$ spectra to the KWW equation and is known as the stretching parameter. In most solid electrolytes, β is typically less than one and it appears that the investigated system exhibits a β value ranging from 0.59 to 0.81 at room temperature. Additionally, the behavior of β appears to be temperature-independent within the studied temperature range, as shown in Fig. 5.16(c) and its inset. The significance of β is that it characterizes the degree of non-exponentially of the relaxation process in the system. A value of β less than one indicates a non-exponential relaxation process, which is often observed in disordered materials or materials with structural heterogeneity. The KWW equation is a common empirical equation used to describe such non-exponential relaxation processes.

According to Ngai [109], it seems that the β value is related to the degree of cooperation between charge carriers during conduction processes in a glass system. A smaller value of β suggests that there is more extensive cooperation between the mobile ions, meaning that when an ion jumps from one equilibrium position to another, it triggers a time-dependent movement of other charge carriers in the surroundings, which results in a further relaxation of the applied electric field. It is noted that the β value varies among different samples, and for all temperatures and among all samples, the obtained value of β for NBP4 is the lowest. This suggests that in the case of NBP4, there is more extensive cooperation between the charge carriers during conduction processes compared to other samples.

Additionally, Jonscher's concept of "universal behavior" [56] suggests that there is a harmonious motion of carriers in a glass, which may be related to the cooperative behavior of charge carriers described by the β value. Finally, Elliot's findings indicate that the jump of a mobile ion in a glass system is not an isolated event, and that it triggers a time-dependent movement of other charge carriers in the surroundings. which results in a further relaxation of the applied electric field. Hence, a smaller value of β results in more extensive

cooperation between charge carriers [110]. A single parallel RC element and a single Maxwell time constant, which Macedo defines as the conductivity relaxation times, are representations of ideal solid electrolytes [60]. In ideal solid electrolytes, $Z^{"}$and $M^{"}$ peak at the same frequency and have the same shape as predicted by the Debye theory for dielectric loss, according to $\omega_{max}\, RC = 1$ [105]. A series of RC elements are taken into account in the case of practical solid electrolytes.

To comprehend the non-Debye behavior of the present system, the impedance and modulus spectra have been displayed at room temperature as shown in Fig. 5.16(d) $Z^{"}_{max}$ and $M^{"}_{max}$do not occur at the same frequency, showing the wide distribution of relaxation times (not obeying mono relaxation time approach), as seen in the graph. West et al;[111] demonstrated that the broadening of the $M^{"}$spectra at high frequencies is due to the spreading of relaxation times, but the substantial increase in the broadening of the $Z^{"}$ spectra at low frequencies is primarily due to electrode polarization. Fig. 5.16(e) shows the actual and imaginary parts of the modulus at $323\, K$ temperature and a concentration of $x = 1\, wt.\%\, NaI$ of the glass composition, in which the relaxation peak of the $M^{"}$spectrum coincides with the corresponding dispersion area in the M' spectra.

Modulus Scaling

The modulus formalism involves the measurement of the real (M') and imaginary ($M^{"}$) components. The $M^{"}$ component is related to the energy dissipation in the material and is therefore a measure of the relaxation processes occurring in the material. The findings of such an investigation indicate that the shape of the $M^{"}$spectra does not vary with temperature variations. This finding suggests that the ionic relaxation mechanism is temperature independent, and that a process known as time-temperature superposition (TTS) holds. TTS is a phenomenon where the relaxation processes occurring at different temperatures can be superimposed onto a single master curve by an appropriate scaling of the $M^{"}$ spectra.

The TTS concept has been widely used in the study of glassy materials and other amorphous solids. It has been widely observed that the shape of the $M^{"}$ spectra is sensitive to variations in the glass composition, and shape of spectra generally increases in width with increasing ion concentration. It supports the hypothesis that the total mobile ion concentration in the glass influences the ion relaxation mechanism.

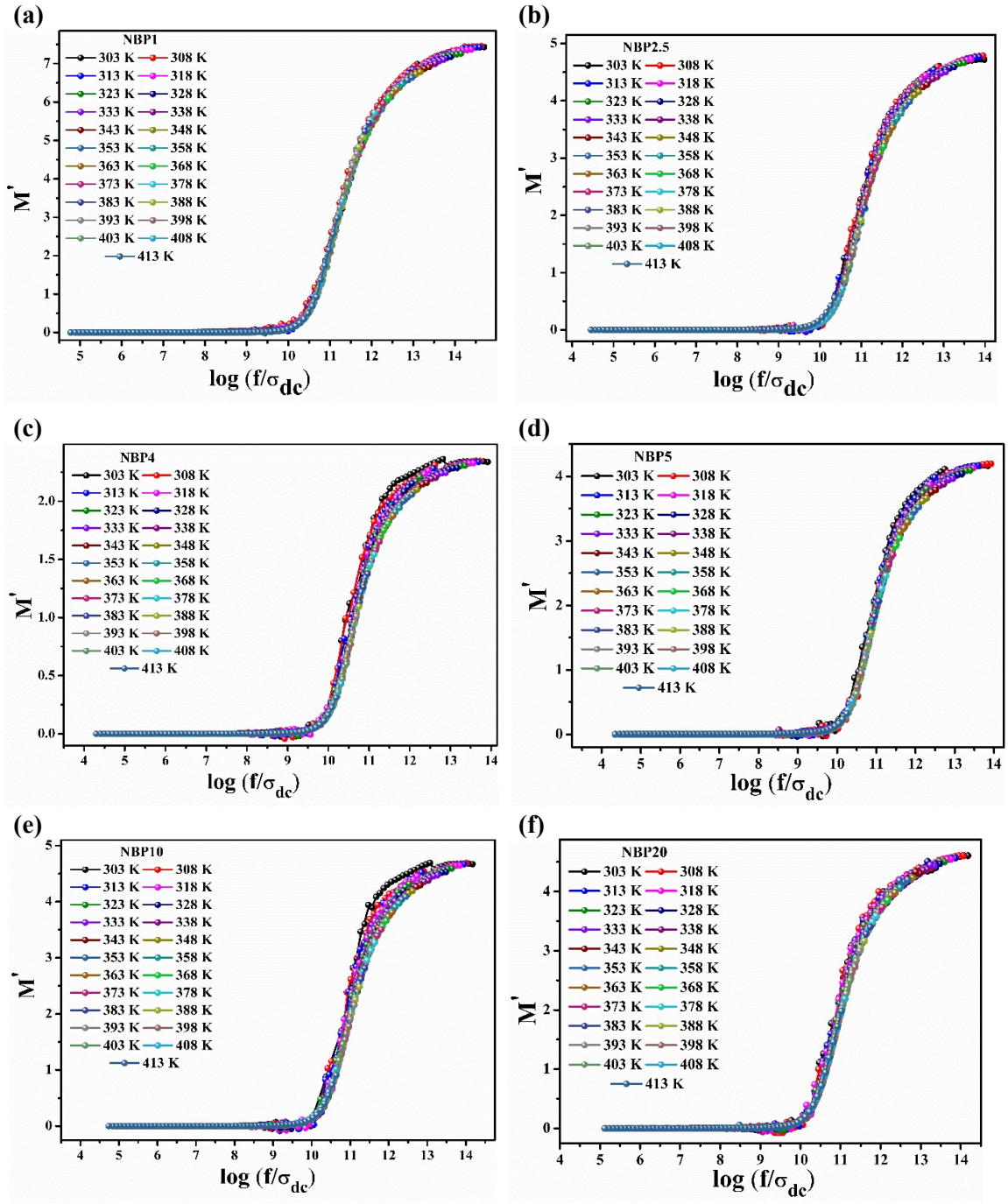

***Figure 5.17**: (a-f) Normalized plots of the real part of the modulus (M') as a function of scaled frequency using Taylor-Isard-Scaling (T-I-S) formalism for all the series samples.*

According to the Taylor-Isard-Scaling (T-I-S) formalism [91], [112], the real component of the modulus is scaled in the current system using the function f/σ_{dc}, while the $M^{"}$ spectrum is scaled using Roling formulation [98], [113] with $M^{"}_{max}$ and its corresponding maximum frequency, f_{max}. Fig. 5.17(a-f) represent the M' vs $\log(f/\sigma_{dc})$ scaling and Fig. 5.18(a-f) depict $M^{"}/M^{"}_{max}$ vs. $\log(f/\sigma_{dc}\,T)$ at various temperatures for all glass compositions.

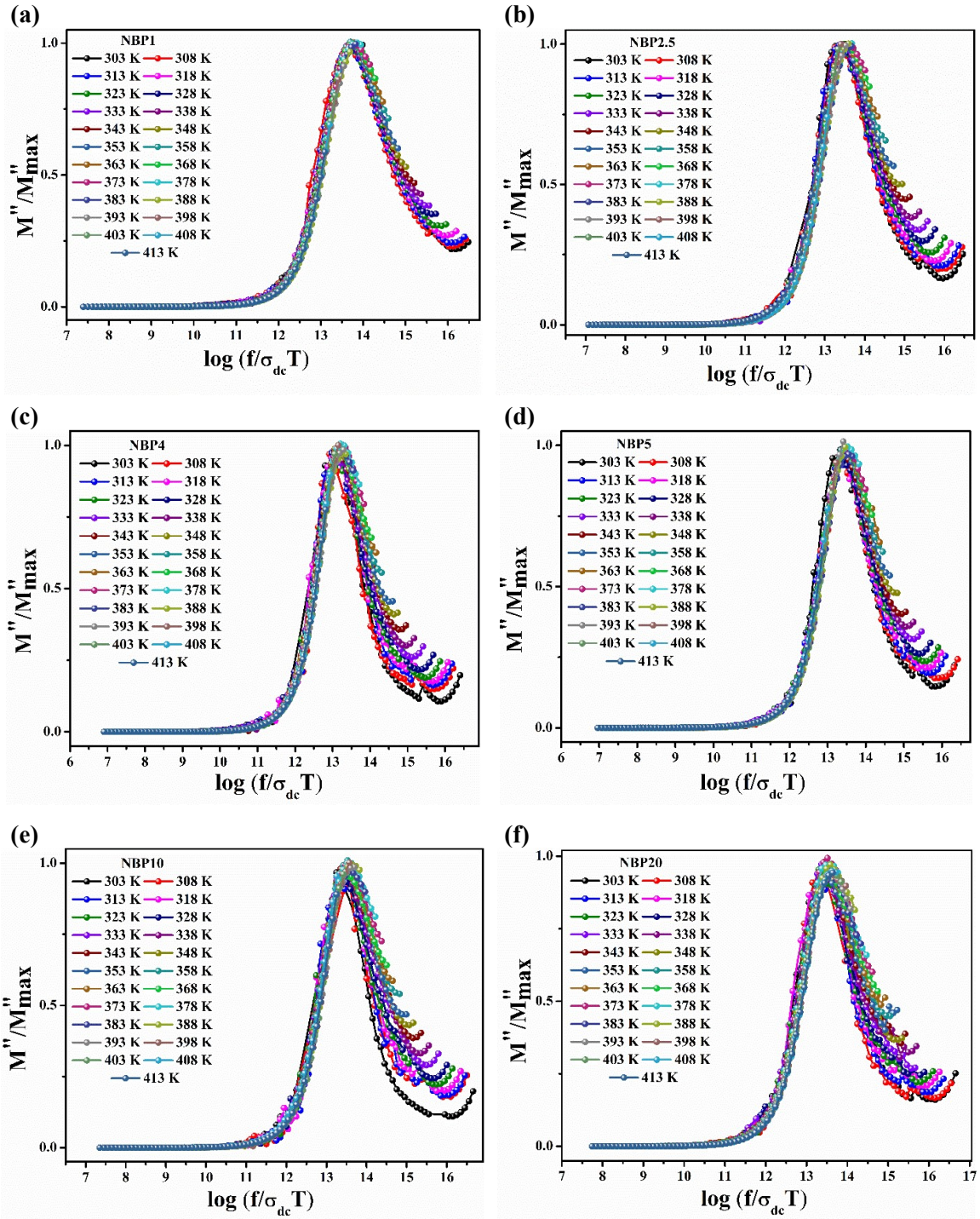

***Figure 5.18**: (a-f) Normalized plots of the imaginary part of the modulus (M'') as a function of scaled frequency using Roling formalism for all the series samples.*

The overlap of the modulus curves at all temperatures suggests that the dynamic processes occurring at different frequencies are not affected by temperature. Furthermore, it is found that the M' and M'' spectra for different temperatures could be integrated into a single "master curve" using T-I-S and Roling formalisms of scaling, respectively, Fig. 5.17(a-f) and Fig. 5.18(a-f).

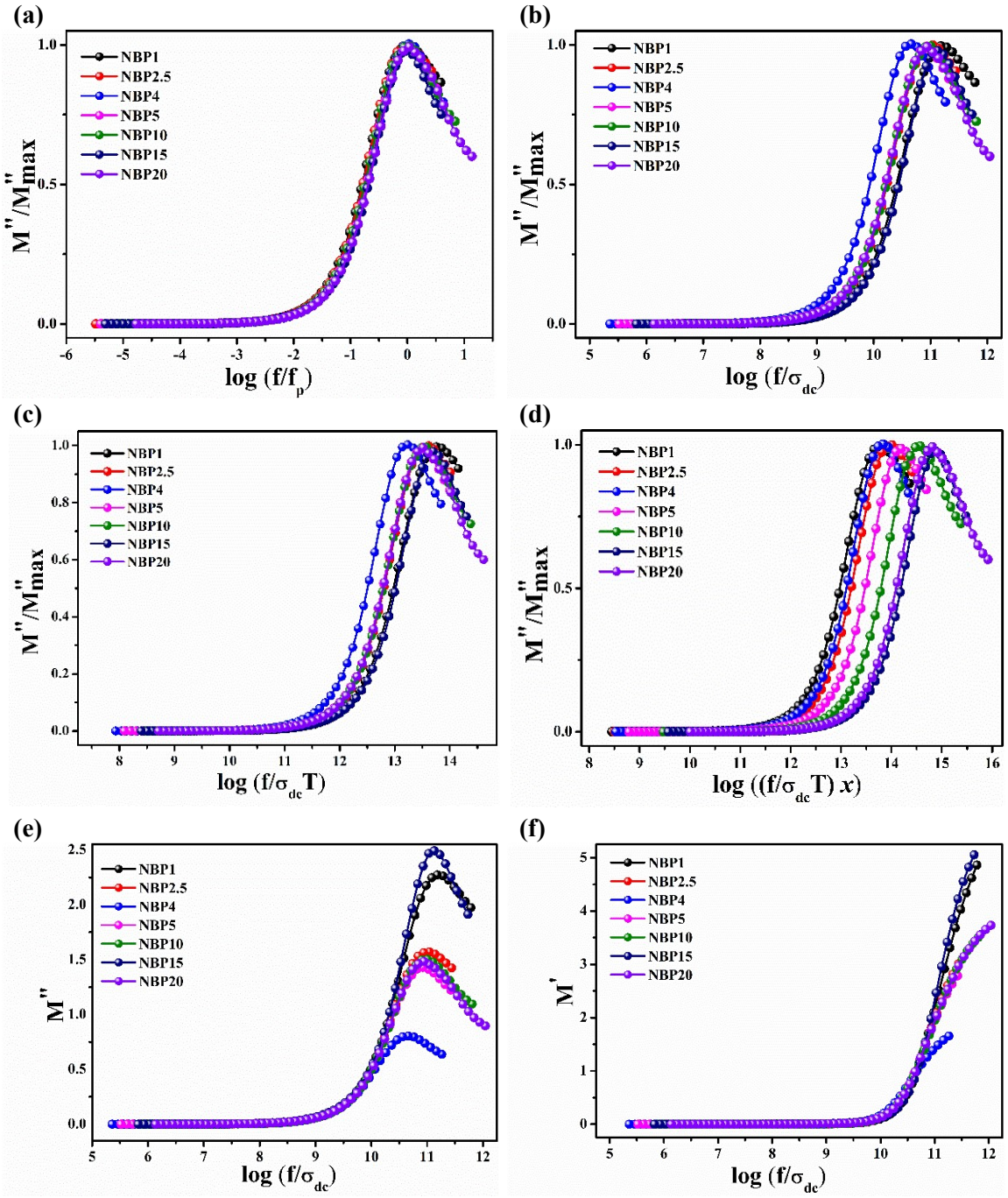

Figure 5.19: *Scaling of imaginary component of modulus for all the glass samples at 373 K temperature using various model formalisms given by (a) Ghosh, (b) Taylor-Isard, (c) Roling and (d) Summerfield. Taylor-Isard formalisms used for (e) imaginary part of modulus* ($M^{"}$)*, and (f) for real part of modulus* (M').

This implies that all dynamic processes occurring at different time scales had the same activation energy and that the distribution of relaxation time was temperature independent. The normalized modulus function, $M^{"}/M^{"}_{max}$, demonstrates a single master curve when scaled with log (f/f_p), according to Ghosh formalism, as depicted in Fig. 5.19(a). After numerous attempts using various scaling formalisms [79]–[81], [112], [114], however,

from Fig. 5.19(b) onward, the imaginary and/or real parts of the modulus do not collapse into a single master curve, particularly at the dispersive frequency region, implying that the relaxation mechanism is affected by changes in glass electrolyte compositions. It also suggests that all dynamic processes occurring at different time scales exhibit the same activation energy and that the distributed relaxation time is independent of temperature.

5.4 Conclusion

In the present study, $\boldsymbol{x(NaI)}: \boldsymbol{(100-x)[30\,Na_2O}: \boldsymbol{(56\,B_2O_3+14\,P_2O_5)]}$ glassy electrolyte, prepared by a rapid melt quench method, the ionic conductivity considerably increases with the addition of NaI up to $4\,wt.\%$ giving a maximum ionic conductivity $1.18883x\ 10^{-8}\ S/cm$ at room temperature. The present borophosphate glass system describes the behavior of borophosphate glasses as electrolytes, specifically their sodium ion conduction mechanism and the nature of their relaxation times as follows.

- The NBP glass system defines the behaviour of borophosphate glasses as electrolytes, in particular the nature of their Na^+ion conduction mechanism and their relaxation durations as the Weak Electrolyte model, as established by Ravaine-Souquet.
- The decoupling index is influenced by the occurrence of trapping effect in NBP glass systems due to relatively smaller size of cations, resulting in an effectively lower concentration of decoupled Na^+ ions at a given temperature.
- The polarisation of an ionic medium at lower frequencies is predominantly governed by the displacement of mobile ions in the direction of the electric field that is applied, seen in the studied range of NaI doped NBP glass samples. The reduction in the magnitude of polarisation or dielectric relaxation strength ($\Delta\varepsilon$) of the medium is a consequence. The dielectric relaxation strength exhibits dependence on both the temperature and glass composition. The observed increase in dielectric relaxation strength ($\Delta\varepsilon$) is attributed to thermal effects and is found to be a gradual function of temperature. The observed polarisation is a result of microscopic phenomena and is susceptible to the effects of mobile ion concentration and hopping distance.
- The electric modulus study confirms that the relaxation times are distributed and non-Debye in nature, with a stretching parameter β that indicates deviation from ideal Debye behaviour. The cooperative nature of the conduction process is

responsible for the distribution of relaxation times in the disordered structure of NBP glasses. A lower value of β in the glass composition indicates greater cooperation among the mobile ions. This means that when an ion moves from one equilibrium position to another, it causes other charge carriers in the vicinity to move in a time-dependent manner, leading to a further relaxation of the applied electric field.

- Additionally, the scaling of conductivity and electric modulus suggests that all dynamic processes in the system have activation energies that are essentially the same. This indicates that the energy required for the system to transition from one state to another is consistent across different timescales. The distribution of relaxation times is also found to be independent of temperature, but is influenced by the glass compositions.

Overall, these findings provide insights into the ion migration process due to presence of varying amount of NaI in disordered structure of sodium borophosphate glass system, emphasizing the importance of cooperative nature of the conduction process which is responsible for the distribution of relaxation times. This suggests that the structure and composition of the glass play a significant role in determining the properties of the electrolyte system.

Bibliography

[1] C. C. Hunter and M. D. Ingram, "Na+-ion conducting glasses," *Solid State Ionics*, vol. 14, no. 1, pp. 31–40, Sep. 1984, doi: 10.1016/0167-2738(84)90007-9.

[2] Y. M. Moustafa and K. El-Egili, "Infrared spectra of sodium phosphate glasses," *J. Non. Cryst. Solids*, vol. 240, no. 1–3, 1998, doi: 10.1016/S0022-3093(98)00711-X.

[3] A. COSTANTINI, A. BURI, and F. BRANDA, "The effect of the substitution of B2O3 to P2O5 on Tg and electrical properties of 0.65 ((1+x) Ag2O P2O5) 0.35 AgI glasses," *Solid State Ionics*, vol. 67, no. 3–4, pp. 175–178, Jan. 1994, doi: 10.1016/0167-2738(94)90001-9.

[4] G. Chiodelli, A. Magistris, and M. Villa, "Ionic conductivity and glass transition of borophosphate glasses," *Solid State Ionics*, vol. 18–19, no. PART 1, pp. 356–361, Jan. 1986, doi: 10.1016/0167-2738(86)90140-2.

[5] A. Magistris, G. Chiodelli, and M. Duclot, "Silver borophosphate glasses : Ion transport, thermal stability and electrochemical behaviour," *Solid State Ionics*, vol. 9–10, no. PART 1, pp. 611–615, 1983, doi: 10.1016/0167-2738(83)90303-X.

[6] T. Tsuchiya and T. Moriya, "Anomalous behavior of physical and electrical properties in borophosphate glasses containing R2O and V2O5," *J. Non. Cryst. Solids*, vol. 38–39, pp. 323–328, May 1980, doi: 10.1016/0022-3093(80)90439-1.

[7] J. F. Ducel and J. J. Videau, "Physical and chemical characterizations of sodium borophosphate glasses," *Mater. Lett.*, vol. 13, no. 4–5, pp. 271–274, Apr. 1992, doi: 10.1016/0167-577X(92)90230-H.

[8] P. S. Anantha and K. Hariharan, "Structure and ionic transport studies of sodium borophosphate glassy system," *Mater. Chem. Phys.*, vol. 89, no. 2–3, pp. 428–437, Feb. 2005, doi: 10.1016/j.matchemphys.2004.09.029.

[9] J. Mizerakova, P. Hockicko, and F. Munoz, "Dielectric Study of Lithium and Sodium Borophosphate Glasses," *Commun. - Sci. Lett. Univ. Zilina*, vol. 19, no. 3, pp. 46–50, Sep. 2017, doi: 10.26552/com.C.2017.3.46-50.

[10] G. Eichinger and G. Deublein, "Fast ionic conduction in sodium phosphate-borate compositions," *Mater. Res. Bull.*, vol. 15, no. 9, pp. 1263–1266, Sep. 1980, doi: 10.1016/0025-5408(80)90029-X.

[11] D. Carta *et al.*, "The effect of composition on the structure of sodium borophosphate glasses," *J. Non. Cryst. Solids*, vol. 354, no. 31, pp. 3671–3677, Aug. 2008, doi: 10.1016/J.JNONCRYSOL.2008.04.009.

[12] M. Schuch, R. Christensen, C. Trott, P. Maass, and S. W. Martin, "Investigation of the Structures of Sodium Borophosphate Glasses by Reverse Monte Carlo Modeling to Examine the Origins of the Mixed Glass Former Effect," *J. Phys. Chem. C*, vol. 116, no. 1, pp. 1503–1511, Jan. 2012, doi: 10.1021/jp2085654.

[13] D. Larink, H. Eckert, M. Reichert, and S. W. Martin, "Mixed network former effect in ion-conducting alkali borophosphate glasses: Structure/property correlations in the system [M2O] 1/3[(B2O3)x(P2O 5)1- X]2/3 (M = Li, K, Cs)," *J. Phys. Chem. C*, vol. 116, no. 50, 2012, doi: 10.1021/jp307085t.

[14] K. H. Sadok, M. Haouari, O. Gallot-Lavallée, and H. Ben Ouada, "Effect of Na2SO4 substitution for Na2O on the structural and electrical properties of a sodium borophosphate glass," *J. Alloys Compd.*, vol. 778, pp. 878–888, Mar. 2019, doi: 10.1016/j.jallcom.2018.11.203.

[15] K. H. Sadok, N. Saad, and M. Haouari, "Physical properties and conductivity relaxation processes in sodium sulfo-borophosphate glasses," *J. Phys. Condens. Matter*, vol. 32, no. 11, p. 115702, Mar. 2020, doi: 10.1088/1361-648X/ab59e9.

[16] R. Suresh Kumar and K. Hariharan, "Ion transport studies in PbI2–Ag2O–V2O5 glassy system," *Solid State Ionics*, vol. 104, no. 3–4, pp. 227–236, Dec. 1997, doi: 10.1016/S0167-2738(97)00419-0.

[17] V. A. Adhwaryu and D. K. Kanchan, "Effect of Lithium Iodide on transport phenomenon in Lithium Borophosphate glass Electrolyte," *J. Non. Cryst. Solids*, vol. 583, p. 121474, May 2022, doi: 10.1016/J.JNONCRYSOL.2022.121474.

[18] F. S. Howell, R. A. Bose, P. B. Macedo, and C. T. Moynihan, "Electrical Relaxation in a Glass-Forming Molten Salt."

[19] H. Mehrer, A. W. Imre, and E. Tanguep-Nijokep, "Diffusion and ionic conduction in oxide glasses," *J. Phys. Conf. Ser.*, vol. 106, no. 1, 2008, doi: 10.1088/1742-6596/106/1/012001.

[20] C. Julien, M. Massot, W. Balkanski, A. Krol, and W. Nazarewicz, "Infrared studies of the structure of borate glasses," *Mater. Sci. Eng. B*, vol. 3, no. 3, pp. 307–312, Aug. 1989, doi: 10.1016/0921-5107(89)90026-3.

[21] R. F. Bartholomew, "Structure and properties of silver phosphate glasses — Infrared and visible spectra," *J. Non. Cryst. Solids*, vol. 7, no. 3, pp. 221–235, Apr. 1972, doi: 10.1016/0022-3093(72)90024-5.

[22] V. N. Rai, B. N. Raja Sekhar, D. M. Phase, and S. K. Deb, "EFFECT OF GAMMA

IRRADIATION ON THE STRUCTURE AND VALENCE STATE OF Nd IN PHOSPHATE GLASS."

[23] Y. M. Lai, X. F. Liang, S. Y. Yang, J. X. Wang, L. H. Cao, and B. Dai, "Raman and FTIR spectra of iron phosphate glasses containing cerium," *J. Mol. Struct.*, vol. 992, no. 1–3, pp. 84–88, Apr. 2011, doi: 10.1016/j.molstruc.2011.02.049.

[24] V. A. Adhwaryu and D. K. Kanchan, "Ag+ ion conduction in AgI-Ag2O-B2O3-P2O5 glass electrolyte," *Mater. Sci. Eng. B Solid-State Mater. Adv. Technol.*, vol. 263, 2021, doi: 10.1016/j.mseb.2020.114857.

[25] A. M. Efimov, "IR fundamental spectra and structure of pyrophosphate glasses along the 2ZnO · P2O5-2Me2O · P2O5 join (Me being Na and Li)," *J. Non. Cryst. Solids*, vol. 209, no. 3, pp. 209–226, 1997, doi: 10.1016/S0022-3093(96)00562-5.

[26] C. Varsamis, "Spectroscopic investigation of AgI-doped borate glasses," *Solid State Ionics*, vol. 136–137, no. 1–2, pp. 1031–1039, Nov. 2000, doi: 10.1016/S0167-2738(00)00557-9.

[27] A. Saranti, I. Koutselas, and M. A. Karakassides, "Bioactive glasses in the system CaO–B2O3–P2O5: Preparation, structural study and in vitro evaluation," *J. Non. Cryst. Solids*, vol. 352, no. 5, pp. 390–398, May 2006, doi: 10.1016/j.jnoncrysol.2006.01.042.

[28] N. J. Kim, S. H. Im, D. H. Kim, D. K. Yoon, and B. K. Ryu, "Structure and properties of borophosphate glasses," *Electron. Mater. Lett.*, vol. 6, no. 3, pp. 103–106, Sep. 2010, doi: 10.3365/eml.2010.09.103.

[29] J. J. Hudgens and S. W. Martin, *Mid-IR and far-IR investigation of AgI-doped silver diborate glasses*, vol. 53, no. 9. 1996, pp. 5348–5355. doi: 10.1103/PhysRevB.53.5348.

[30] M. Htut, M. Lwin, P. Kaung, and S. Htoon, *No Title*, vol. IV, no. 2. 2006. [Online]. Available: http://www.iaea.org/inis/collection/NCLCollectionStore/_Public/40/057/40057374.pdf

[31] C. Calahoo and L. Wondraczek, "Ionic glasses: Structure, properties and classification," *J. Non-Crystalline Solids X*, vol. 8, p. 100054, 2020, doi: 10.1016/j.nocx.2020.100054.

[32] B. K. Money and K. Hariharan, "Glass formation and electrical conductivity studies of melt quenched and mechanically milled 50Li2O:(50−x) P2O5:xB2O3," *Solid State Ionics*, vol. 179, no. 27–32, pp. 1273–1277, Sep. 2008, doi: 10.1016/j.ssi.2007.12.068.

[33] T. Q. & M. Leow, T. & I. Leong & Eeu, Zuhairi & Hussin, and Rosli, "Study of Structural and Luminescence Properties of Lead Lithium Borophosphate Glass System Doped with Ti Ions. Sains Malaysiana. 43. 929-934. ," *Sains Malaysiana.* , vol. 43., pp. 929-934., 2014.

[34] W. M. Hua, P. S. Wong, R. Hussin, and Z. Ibrahim, "Structural Study on Lithium-Barium Borophosphate Glasses Using Infrared and Raman Spectroscopy," *Adv. Mater. Res.*, vol. 626, pp. 11–15, Dec. 2012, doi: 10.4028/www.scientific.net/AMR.626.11.

[35] C. Gautam, A. K. Yadav, and A. K. Singh, "A Review on Infrared Spectroscopy of Borate Glasses with Effects of Different Additives," *ISRN Ceram.*, vol. 2012, pp. 1–17, 2012, doi: 10.5402/2012/428497.

[36] H. A. Othman, H. S. Elkholy, and I. Z. Hager, "FTIR of binary lead borate glass: Structural investigation," *J. Mol. Struct.*, vol. 1106, pp. 286–290, Feb. 2016, doi: 10.1016/j.molstruc.2015.10.076.

[37] D. Toloman *et al.*, "Phosphate Glassy Network Depolymerization Induced by CaO Doping," *Part. Sci. Technol.*, vol. 28, no. 3, pp. 226–235, May 2010, doi: 10.1080/02726351.2010.481581.

[38] J.-O. Byun, B.-H. Kim, K.-S. Hong, H.-J. Jung, S.-W. Lee, and A. A. Izyneev, "Properties and structure of RO□Na2O□Al2O3□P2O5 (R = Mg, Ca, Sr, Ba) glasses," *J. Non. Cryst. Solids*, vol. 190, no. 3, pp. 288–295, Oct. 1995, doi: 10.1016/0022-3093(95)00280-4.

[39] C. Dayanand, G. Bhikshamaiah, V. J. Tyagaraju, M. Salagram, and A. S. R. Krishna Murthy, "Structural investigations of phosphate glasses: a detailed infrared study of the x(PbO)-(1−x) P2O5 vitreous system," *J. Mater. Sci.*, vol. 31, no. 8, pp. 1945–1967, Apr. 1996, doi: 10.1007/BF00356615.

[40] THIEU DUC THO, "ION CONDUCTION MECHANISMS IN FAST ION CONDUCTING OXIDE GLASSES FOR RECHARGEABLE BATTERIES," NATIONAL UNIVERSITY OF SINGAPORE, 2011.

[41] X. Zhang and M. Cresswell, "Materials Characterization of Inorganic Controlled Release," *Inorg. Control. Release Technol.*, pp. 57–91, Jan. 2016, doi: 10.1016/B978-0-08-099991-3.00003-X.

[42] M. Moutataouia *et al.*, "Structural Investigation of Bi2o3-P2o5-B2o3 -V2o5 Quaternary Glass System by Raman, Ftir and Thermal Analysis," *SSRN Electron. J.*, 2020, doi: 10.2139/ssrn.3621129.

[43] P. Machowski, J. E. Garbarczyk, and M. Wasiucionek, "Impedance spectra of mixed conductive silver vanadate-phosphate glasses," *Solid State Ionics*, vol. 157, no. 1–4, pp. 281–285, Feb. 2003, doi: 10.1016/S0167-2738(02)00222-9.

[44] A. Moguš-Milanković *et al.*, "Electrical, dielectric and spectroscopic studies on MnO doped

LiI-AgI-B 2O 3 glasses," *J. Appl. Phys.*, vol. 111, no. 1, pp. 0–11, 2012, doi: 10.1063/1.3676254.

[45] B.-A. Mei, J. Lau, T. Lin, S. H. Tolbert, B. S. Dunn, and L. Pilon, "Physical Interpretations of Electrochemical Impedance Spectroscopy of Redox Active Electrodes for Electrical Energy Storage," *J. Phys. Chem. C*, vol. 122, no. 43, pp. 24499–24511, Nov. 2018, doi: 10.1021/acs.jpcc.8b05241.

[46] A. K. Jonscher, "Analysis of the alternating current properties of ionic conductors," *J. Mater. Sci.*, vol. 13, no. 3, pp. 553–562, Mar. 1978, doi: 10.1007/BF00541805.

[47] N. Satyanarayana, A. Karthikeyan, and M. Venkateswarlu, "A.c. conductivity studies on the silver molybdo-arsenate glassy system," *J. Mater. Sci.*, vol. 31, no. 20, pp. 5471–5477, 1996, doi: 10.1007/BF01159319.

[48] D. . S. J. . Ravaine, "A thermodynamic approach to ionic conductivity in oxide glasses.," *Phys. Chem. Glas.*, vol. 18, no. 27, 1977.

[49] J. O. Isard, "The mixed alkali effect in glass," *J. Non. Cryst. Solids*, vol. 1, no. 3, pp. 235–261, Apr. 1969, doi: 10.1016/0022-3093(69)90003-9.

[50] J. O. Isard, "The Haven ratio in glasses," *J. Non. Cryst. Solids*, vol. 246, no. 1–2, pp. 16–26, Apr. 1999, doi: 10.1016/S0022-3093(99)00036-8.

[51] C. T. MOYNIHAN and A. V. LESIKAR, "Weak-Electrolyte Models for the Mixed-Alkali Effect in Glass," *J. Am. Ceram. Soc.*, vol. 64, no. 1, pp. 40–46, Jan. 1981, doi: 10.1111/j.1151-2916.1981.tb09556.x.

[52] R. Christensen, G. Olson, and S. W. Martin, "Ionic conductivity of mixed glass former 0.35Na2O + 0.65[x B2O3 + (1 - X)P2O5] glasses," *J. Phys. Chem. B*, vol. 117, no. 51, 2013, doi: 10.1021/jp409497z.

[53] S. W. Martin and C. A. Angell, "Dc and ac conductivity in wide composition range Li2OP2O5 glasses," *J. Non. Cryst. Solids*, vol. 83, no. 1–2, 1986, doi: σ_(523-623)≈〖10〗^(-8)-〖10〗^(-3).

[54] C. A. Angell, *MOBILE IONS IN AMORPHOUS SOLIDS*, vol. 43, no. 1. Annual Reviews, 1992, pp. 693–717. doi: 10.1146/annurev.physchem.43.1.693.

[55] M. Pollak and T. H. Geballe, "Low-Frequency Conductivity Due to Hopping Processes in Silicon," *Phys. Rev.*, vol. 122, no. 6, pp. 1742–1753, Jun. 1961, doi: 10.1103/PhysRev.122.1742.

[56] A. K. Jonscher, "The 'universal' dielectric response," *Nature*, vol. 267, no. 5613, pp. 673–679, Jun. 1977, doi: 10.1038/267673a0.

[57] K. L. Ngai and C. T. White, "Frequency dependence of dielectric loss in condensed matter," *Phys. Rev. B*, vol. 20, no. 6, pp. 2475–2486, Sep. 1979, doi: 10.1103/PhysRevB.20.2475.

[58] L. A. Dissado and R. M. Hill, "Non-exponential decay in dielectrics and dynamics of correlated systems," *Nature*, vol. 279, no. 5715, pp. 685–689, Jun. 1979, doi: 10.1038/279685a0.

[59] B. CHOWDARI and R. GOPALAKRISHNAN, "ac conductivity analysis of glassy silver iodomolybdate system☆," *Solid State Ionics*, vol. 23, no. 3, pp. 225–233, Apr. 1987, doi: 10.1016/0167-2738(87)90055-5.

[60] P. B. Macedo, C. T. Moynihan, and R. Bose, "The Role of Ionic Diffusion in Polarization in Vitreous Ionic.," *Phys. Chem. Glas.*, vol. 13, no. 6, pp. 171–179, 1972.

[61] M. Ganguli, M. H. Bhat, and K. J. Rao, "Role of PbO in lithium ion transport in Li2O–PbO–B2O3 glasses," *Mater. Res. Bull.*, vol. 34, no. 10–11, pp. 1757–1772, Jul. 1999, doi: 10.1016/S0025-5408(99)00154-3.

[62] M. D. Ingram, "Ionic Conductivity in Glass," *Phys. Chem. Glas.*, pp. 214–234, 1987.

[63] A. K. Jonscher, "A new understanding of the dielectric relaxation of solids," *J. Mater. Sci.*, vol. 16, no. 8, pp. 2037–2060, Aug. 1981, doi: 10.1007/BF00542364.

[64] M. Dult, R. S. Kundu, S. Murugavel, R. Punia, and N. Kishore, "Conduction mechanism in bismuth silicate glasses containing titanium," *Phys. B Condens. Matter*, vol. 452, pp. 102–107, Nov. 2014, doi: 10.1016/j.physb.2014.07.004.

[65] K. H. Mahmoud, F. M. Abdel-Rahim, K. Atef, and Y. B. Saddeek, "Dielectric dispersion in lithium–bismuth-borate glasses," *Curr. Appl. Phys.*, vol. 11, no. 1, pp. 55–60, Jan. 2011, doi: 10.1016/j.cap.2010.06.018.

[66] S. Renka *et al.*, "A significant enhancement of sodium ion conductivity in phosphate glasses by addition of WO_3 and MoO_3 : the effect of mixed conventional–conditional glass-forming oxides," *Phys. Chem. Chem. Phys.*, vol. 23, no. 16, pp. 9761–9772, 2021, doi: 10.1039/D1CP00498K.

[67] N. Chakchouk, B. Louati, and K. Guidara, "Electrical properties and conduction mechanism study by OLPT model of NaZnPO4 compound," *Mater. Res. Bull.*, vol. 99, pp. 52–60, Mar. 2018, doi: 10.1016/j.materresbull.2017.10.046.

[68] K. Funke, "Debye-Hückel-Type Relaxation Processes in Solid Ionic Conductors," *Zeitschrift für Phys. Chemie*, vol. 154, no. 1–2, pp. 251–295, Jan. 1987, doi: 10.1524/zpch.1987.154.Part_1_2.251.

[69] K. Funke, "Jump relaxation in solid ionic conductors," *Solid State Ionics*, vol. 28–30, no. PART 1, pp. 100–107, 1988, doi: 10.1016/S0167-2738(88)80015-8.

[70] D. ALMOND and A. WEST, "Mobile ion concentrations in solid electrolytes from an analysis of a.c. conductivity," *Solid State Ionics*, vol. 9–10, pp. 277–282, Dec. 1983, doi: 10.1016/0167-2738(83)90247-3.

[71] D. P. Almond, A. R. West, and R. J. Grant, "Temperature dependence of the a.c. conductivity of Naβ-alumina," *Solid State Commun.*, vol. 44, no. 8, pp. 1277–1280, Nov. 1982, doi: 10.1016/0038-1098(82)91103-6.

[72] D. P. Almond and A. R. West, "Impedance and modulus spectroscopy of 'real' dispersive conductors," *Solid State Ionics*, vol. 11, no. 1, pp. 57–64, Sep. 1983, doi: 10.1016/0167-2738(83)90063-2.

[73] A. K. Jonscher, "Dielectric relaxation in solids," *J. Phys. D. Appl. Phys.*, vol. 32, no. 14, pp. R57–R70, Jul. 1999, doi: 10.1088/0022-3727/32/14/201.

[74] D. P. Almond and A. R. West, "Comments on the analyses of AC conductivity data for single crystal Na β-alumina at low temperatures," *J. Electroanal. Chem.*, vol. 193, no. 1–2, pp. 49–55, Oct. 1985, doi: 10.1016/0022-0728(85)85051-8.

[75] H. Kahnt, "Ionic Transport in Oxide Glasses and Frequency Dependence of Conductivity," *Berichte der Bunsengesellschaft für Phys. Chemie*, vol. 95, no. 9, pp. 1021–1025, Sep. 1991, doi: 10.1002/bbpc.19910950913.

[76] A. Pan and A. Ghosh, *Activation energy and conductivity relaxation of sodium tellurite glasses*, vol. 59, no. 2. 1999, pp. 899–904. doi: 10.1103/PhysRevB.59.899.

[77] A. Kulkarni, "Scaling behaviour in the frequency dependent conductivity of mixed alkali glasses," *Solid State Ionics*, vol. 112, no. 1–2, pp. 69–74, Sep. 1998, doi: 10.1016/S0167-2738(98)00210-0.

[78] Á. W. Imre, S. Voss, and H. Mehrer, "Ionic transport in 0.2[XNa2O·(1–X)Rb2O]·0.8B2O3 mixed-alkali glasses," *Phys. Chem. Chem. Phys.*, vol. 4, no. 14, pp. 3219–3224, Jul. 2002, doi: 10.1039/b110980b.

[79] S. Summerfield, "Universal low-frequency behaviour in the a.c. hopping conductivity of disordered systems," *Philos. Mag. B Phys. Condens. Matter; Stat. Mech. Electron. Opt.*

Magn. Prop., vol. 52, no. 1, pp. 9–22, 1985, doi: 10.1080/13642818508243162.

[80] B. Roling, A. Happe, K. Funke, and M. D. Ingram, "Carrier Concentrations and Relaxation Spectroscopy: New Information from Scaling Properties of Conductivity Spectra in Ionically Conducting Glasses," *Phys. Rev. Lett.*, vol. 78, no. 11, pp. 2160–2163, Mar. 1997, doi: 10.1103/PhysRevLett.78.2160.

[81] A. Ghosh and A. Pan, *Scaling of the conductivity spectra in ionic glasses: Dependence on the structure*, vol. 84, no. 10. 2000, pp. 2188–2190. doi: 10.1103/PhysRevLett.84.2188.

[82] J. C. Dyre, P. Maass, B. Roling, and D. L. Sidebottom, "Fundamental questions relating to ion conduction in disordered solids," *Reports Prog. Phys.*, vol. 72, no. 4, 2009, doi: 10.1088/0034-4885/72/4/046501.

[83] D. L. Sidebottom and J. Zhang, *Scaling of the ac permittivity in ion-conducting glasses*, vol. 62, no. 9. 2000, pp. 5503–5507. doi: 10.1103/PhysRevB.62.5503.

[84] D. L. Sidebottom, "Colloquium: Understanding ion motion in disordered solids from impedance spectroscopy scaling," *Rev. Mod. Phys.*, vol. 81, no. 3, pp. 999–1014, Aug. 2009, doi: 10.1103/RevModPhys.81.999.

[85] M. Bettman and C. R. Peters, "Crystal structure of Na2O.MgO.5Al2O3 [sodium oxide-magnesia-alumina] with reference to Na2O.5Al2O3 and other isotypal compounds," *J. Phys. Chem.*, vol. 73, no. 6, pp. 1774–1780, Jun. 1969, doi: 10.1021/j100726a024.

[86] K. Funke, "Ionic conductivity of α-RbAg4I5 up to far-infrared frequencies," *Solid State Ionics*, vol. 13, no. 4, pp. 335–343, Aug. 1984, doi: 10.1016/0167-2738(84)90077-8.

[87] K. Funke, R. D. Banhatti, D. Wilmer, R. Dinnebier, A. Fitch, and M. Jansen, "Low-Temperature Phases of Rubidium Silver Iodide: Crystal Structures and Dynamics of the Mobile Silver Ions," *J. Phys. Chem. A*, vol. 110, no. 9, pp. 3010–3016, Mar. 2006, doi: 10.1021/jp054807v.

[88] M. Vogel, C. Brinkmann, H. Eckert, and A. Heuer, "Origin of nonexponential relaxation in a crystalline ionic conductor: A multidimensional 109Ag NMR study," *Phys. Rev. B - Condens. Matter Mater. Phys.*, vol. 69, no. 9, 2004, doi: 10.1103/PhysRevB.69.094302.

[89] I. Svare, *Conductivity and NMR relaxation from ionic motion in disordered glasses with distributions of barriers*, vol. 125, no. 1. Elsevier Science Publishers B.V., 1999, pp. 47–53. doi: 10.1016/S0167-2738(99)00157-5.

[90] K. S. Cole and R. H. Cole, "Dispersion and Absorption in Dielectrics I. Alternating Current Characteristics," *J. Chem. Phys.*, vol. 9, no. 4, pp. 341–351, Apr. 1941, doi:

10.1063/1.1750906.

[91] J. C. Dyre and T. B. Schroøder, “Universality of ac conduction in disordered solids,” *Rev. Mod. Phys.*, 2000, doi: 10.1103/RevModPhys.72.873.

[92] B. CHOWDARI and R. GOPALAKRISHNAN, “Impedance and modulus spectroscopy of vitreous AgI□Ag2O□P2O5 system,” *Solid State Ionics*, vol. 18–19, pp. 483–487, Jan. 1986, doi: 10.1016/0167-2738(86)90164-5.

[93] R. Kaushik, K. Hariharan, and S. Radhakrishna, “Transport studies on thin films of Ag7I4VO4 solid electrolyte,” *J. Appl. Electrochem.*, vol. 17, no. 4, pp. 813–820, Jul. 1987, doi: 10.1007/BF01007819.

[94] R. D. Armstrong and K. Taylor, “The impedance of solid electrolyte cells over the frequency range 10−3 to 108 Hz,” *J. Electroanal. Chem. Interfacial Electrochem.*, vol. 63, no. 1, pp. 9–17, Jul. 1975, doi: 10.1016/S0022-0728(75)80121-5.

[95] G. Cochrane and N. H. Fletcher, “Ionic conductivity and low frequency dispersion in hexagonal silver iodide,” *J. Phys. Chem. Solids*, vol. 32, no. 11, pp. 2557–2567, Jan. 1971, doi: 10.1016/S0022-3697(71)80102-6.

[96] M. V. Šušić and S. V. Mentus, “Electrochemical behaviour of the solid electrolyte Ag6I4WO4,” *Electrochim. Acta*, vol. 28, no. 1, pp. 35–41, Jan. 1983, doi: 10.1016/0013-4686(83)85084-1.

[97] S. A. SUTHANTHIRARAJ and S. RADHAKRISHNA, “Transport studies on thin films of Ag6I4MoO4 solid electrolyte,” *Cryst. lattice defects Amorph. Mater.*, vol. 11, no. 3, pp. 185–195, 1985.

[98] T. B. Schrøder and J. C. Dyre, “Scaling and universality of ac conduction in disordered solids,” *Phys. Rev. Lett.*, vol. 84, no. 2, pp. 310–313, 2000, doi: 10.1103/PhysRevLett.84.310.

[99] E. Barsoukov and J. R. Macdonald, Eds., *Impedance Spectroscopy*. Wiley, 2005. doi: 10.1002/0471716243.

[100] M. Venkateswarlu, “A.c. conductivity and dielectric studies of silver-based fast ion conducting glass system,” *Solid State Ionics*, vol. 127, no. 1–2, pp. 177–184, Jan. 2000, doi: 10.1016/S0167-2738(99)00257-X.

[101] A. S. Nowick and B. S. Lim, “Analysis of ac conductivity data for Na2O·3SiO2 glass by stretched exponential and Jonscher power-law methods,” *J. Non. Cryst. Solids*, vol. 172–174, no. PART 2, pp. 1389–1394, Sep. 1994, doi: 10.1016/0022-3093(94)90667-X.

[102] M. Sural and A. Ghosh, “Conductivity relaxation in zirconium fluoride glasses: effect of substitution of Zr4+ by Y3+ ions,” *Solid State Ionics*, vol. 120, no. 1–4, pp. 27–32, May 1999, doi: 10.1016/S0167-2738(98)00551-7.

[103] M. Pant, D. K. Kanchan, P. Sharma, and M. S. Jayswal, “Mixed conductivity studies in silver oxide based barium vanado–tellurite glasses,” *Mater. Sci. Eng. B*, vol. 149, no. 1, pp. 18–25, Mar. 2008, doi: 10.1016/j.mseb.2007.11.037.

[104] W. . Hasz, C. . Moynihan, and P. . Tick, “Electrical relaxation in a CdF2□LiF□AlF3□PbF2 glass and melt,” *J. Non. Cryst. Solids*, vol. 172–174, pp. 1363–1372, Sep. 1994, doi: 10.1016/0022-3093(94)90664-5.

[105] R. J. GRANT, M. D. INGRAM, and A. R. WEST, “AN INVESTIGATION OF β-ALUMINA ELECTROLYTES BY ELECTRIC MODULUS SPECTROSCOPY,” in *International Symposium on Solid Ionic and Ionic-Electronic Conductors*, Elsevier, 1977, pp. 729–734. doi: 10.1016/B978-0-08-021592-1.50016-7.

[106] R. Kohlrausch, “Ueber das Dellmann’sche Elektrometer,” *Ann. der Phys. und Chemie*, vol. 148, no. 11, pp. 353–405, 1847, doi: 10.1002/andp.18471481102.

[107] C. T. Moynihan, “Analysis of electrical relaxation in glasses and melts with large concentrations of mobile ions,” Sep. 1994. doi: 10.1016/0022-3093(94)90668-8.

[108] G. Williams and D. C. Watts, “Non-symmetrical dielectric relaxation behaviour arising from a simple empirical decay function,” *Trans. Faraday Soc.*, vol. 66, p. 80, 1970, doi: 10.1039/tf9706600080.

[109] K. L. Ngai, J. N. Mundy, H. Jain, O. Kanert, and G. Balzer-Jollenbeck, “Correlation between the activation enthalpy and Kohlrausch exponent for ionic conductivity in alkali aluminogermanate glasses,” *Phys. Rev. B*, vol. 39, no. 9, pp. 6169–6179, Mar. 1989, doi: 10.1103/PhysRevB.39.6169.

[110] S. ELLIOTT, “Frequency-dependent conductivity in ionically and electronically conducting amorphous solids,” *Solid State Ionics*, vol. 70–71, pp. 27–40, May 1994, doi: 10.1016/0167-2738(94)90284-4.

[111] A. R. WEST, D. C. SINCLAIR, and N. HIROSE, “Characterization of Electrical Materials, Especially Ferroelectrics, by Impedance Spectroscopy,” *J. Electroceramics*, vol. 1, no. 1, pp. 65–71, 1997, doi: 10.1023/A:1009950415758.

[112] J. O. Isard, “A study of the migration loss in glass and a generalized method of calculating the rise of dielectric loss with temperature,” *Proc. IEE - Part B Electron. Commun. Eng.*,

vol. 109, no. 22S, pp. 440–447, 1962, doi: 10.1049/pi-b-2.1962.0077.

[113] B. Roling, *What do electrical conductivity and electrical modulus spectra tell us about the mechanisms of ion transport processes in melts, glasses, and crystals?*, vol. 244, no. 1. Elsevier, 1999, pp. 34–43. doi: 10.1016/S0022-3093(98)00847-3.

[114] A. Pan and A. Ghosh, *Relaxation dynamics of lithium ions in lead bismuthate glasses*, vol. 62, no. 5. 2000, pp. 3190–3195. doi: 10.1103/PhysRevB.62.3190.